



Assessment of mudflow risk in Uzbekistan using CMIP5 models

Gavkhar Mamadjanova^{a,b,c,*}, Gregor C. Leckebusch^{a,d}

^a School of Geography, Earth and Environmental Sciences, University of Birmingham, Birmingham, B15 2TT, UK

^b Department of Hydrometeorology, National University of Uzbekistan, Tashkent, 100174, Uzbekistan

^c Hydrometeorological Research Institute, Center of Hydrometeorological Service of the Republic of Uzbekistan (Uzhydromet), Tashkent, 100052, Uzbekistan

^d Institute for Meteorology, FU Berlin, 12165, Berlin, Germany

ARTICLE INFO

Keywords:

CMIP5
Circulation weather types
Large-scale circulation
Landslides
Mudflows
Precipitation threshold
Global warming impact
Uzbekistan

ABSTRACT

Precipitation induced mudflows are a major and longstanding threat in Uzbekistan, impacting on many properties and livelihoods. In this paper, the role of large-scale atmospheric circulation in producing the conditions necessary to initiate mudflows in piedmont areas of Uzbekistan have been evaluated based on historical and scenario (Representative Concentration Pathways; RCP8.5) experiments along from 10 Coupled Model Inter-comparison Project Phase 5 (CMIP5) models. Applying the well-established circulation weather type (CWT) technique, and CMIP5 models reveal that mudflow generating large-scale circulation flows will increase by up to 5% to the end of the century. Considering the historical simulations over 1979–2005 and following the projections of RCP8.5 emission scenario for the target period of 2071–2100, precipitation climatology has been evaluated using bias correction techniques. By this way, the synthetic rainfall series were linked to a central proxy – a mudflow generating weather types, such as cyclonic (C), westerly (W) and south-westerly (SW) in order to diagnose potential changes in mudflow occurrences given the changed CWT characteristics by running the statistical-empirical algorithm of antecedent daily rainfall model (ADRM) and statistical logistic regression (LRM). Results for the important weather types (C, W and SW) confirm that mudflow activity will increase in the selected region as precipitation values associated with the CWT C and W flows in CMIP5 projections are expected to increase in the warm season for the target period of 2071–2100.

The research focuses on piedmont areas of Uzbekistan as it has remained poorly understood due to limited climate research, particularly, in mountain areas. This is important in the face of climate change, which is likely to increase pressure upon high mountain areas that may need to investigate more frequent mudflow occurrences.

1. Introduction

In the last 15 years, more than 50 people died, many properties destroyed, and livelihoods threatened due to precipitation induced mudflow occurrences in Uzbekistan (source Uzhydromet¹). Also, a large part of the country is involved in agriculture making it very vulnerable to hydrometeorological disasters. With the population forecasted to grow over the rest of this century (UN report²) and associated increase in human settlements and land use activities in the piedmont and mountain zones of Uzbekistan, it is important, that the complex weather phenomena and their impacts over the country is investigated considering various global warming scenarios.

Future projections of anthropogenic climate change have focused on

surface temperatures and precipitation characteristics over the Central Asian region, which includes Uzbekistan. For instance, Ozturk et al. (2012, 2017) investigated the impact of climate change results on seasonal variability of precipitation and temperature over Central Asia under the framework of Coordinated Regional Climate Downscaling Experiment (CORDEX) Region 8 by using RegCM4 and RegCM4.3.5. Results obtained from the regional RegCM4 model driven by the ECHAM5 A1B scenario for the future (2070–2100) climatology of Central Asia show relatively high warming trend in surface temperature (from 3 °C up to 11.4 °C on average) and a decrease in precipitation, particularly, in the south-eastern part of the domain (Ozturk et al., 2012). RCP4.5 and RCP8.5 scenarios of the HadGEM2-ES and the MPI-ESM-MR models downscaled by the RegCM4.3.5 climate projection

* Corresponding author. School of Geography, Earth and Environmental Sciences, University of Birmingham, Birmingham, B15 2TT, UK.

E-mail address: G.Mamadjanova@bham.ac.uk (G. Mamadjanova).

¹ Centre of Hydrometeorological Service of the Republic of Uzbekistan.

² <https://population.un.org/wpp/Graphs/Probabilistic/POP/TOT/860>.

<https://doi.org/10.1016/j.wace.2021.100403>

Received 5 June 2021; Received in revised form 28 October 2021; Accepted 29 November 2021

Available online 30 November 2021

2212-0947/© 2021 The Authors. Published by Elsevier B.V. This is an open access article under the CC BY license (<http://creativecommons.org/licenses/by/4.0/>).

for near future (2011–2040), mid-future (2041–2070) and far future (2071–2100) in [Ozturk et al. \(2017\)](#) also show reasonably good agreement with the outputs of previous study by [Ozturk et al. \(2012\)](#).

The high-resolution regional climate model (RCM) REMO has been implemented over Central Asia by [Mannig et al. \(2013\)](#) in order to better understand the seasonal cycle of precipitation and temperature under the anthropogenic climate change. Downscaled ECHAM5/MPI-OM A1B emission scenario indicates a warming of up to 7 °C in the northern part of Central Asia and mountain areas until the end of the twenty-first century. However, climate change scenarios predict dryer summer conditions in a large area of Central Asia and wetter cold seasons over the northern part of the region and for most areas of the Tibetan Plateau.

[Huang et al. \(2014\)](#) projected future change in the annual precipitation over Central Asia for the period 2011–2100 by applying CMIP5 ([Taylor et al., 2012](#)) GCMs under the different emission scenarios (RCP2.6, RCP4.5 and RCP8.5). The authors found increasing trends in annual precipitation (over 3–9 mm per decade) for the northern Central Asia, the Tian-Shan Mountains and northern Tibet by the end of 2100 when they compared with the previous investigations on climate change signals over the Central Asia. The authors suggested that large scale atmospheric water vapour fluxes and surface evaporation over the study region could be the possible mechanisms of the increasing changes in projected precipitation ([Huang et al., 2014](#)).

In many studies ([Sorg et al., 2012, 2014](#); [Kure et al., 2013](#)) the adverse effects of global warming to the Central Asian glacier zones have been evaluated. Researchers have predicted a substantial glacier shrinkage due to the increase in air temperature over the Tien Shan and the Pamir Mountains, considered to be the water tower of Central Asia and its effects on the water availability until the end of the century. Using the recent developments in the field of climate modelling, [Malsy et al. \(2012\)](#), [White et al. \(2014\)](#) and [Radchenko et al. \(2017\)](#) investigated the impact of climate change on water resources in Central Asia, including Uzbekistan. Moreover, increased risks due to climate change and its negative consequences on agriculture and food productivity over Central Asia have been investigated by employing Crop Syst and DSSAT crop modelling approach ([Sommer et al., 2013](#); [Bobojonov and Aw-Hassan, 2014](#)).

These studies aside, there have been relatively few investigations focusing on the projected changes in large scale atmospheric circulation as a main driver of precipitation extremes over Central Asia under global warming conditions. [Zhao et al. \(2018\)](#) simulated subtropical westerly jet (SWJ) stream and its effect on the projected precipitation over Central Asia for the summers of 2071–2100 by using of 25 CMIP5 models. By applying the empirical orthogonal function (EOF) method, these authors revealed the strength and position of SWJ over Central Asia in the future. According to the ensemble results from CMIP5, [Zhao et al. \(2018\)](#) explained the SWJ axis shifting further south over Central Asia which will result in more summer rainfall in most of northern and north-eastern part of the region in the future, however, the authors found uncertainties regarding future precipitation changes in the rest of the Central Asia.

Hitherto only [Reyers et al. \(2013\)](#) studied the link between weather system and precipitation frequency and its magnitude for the Aksu river basin in Central Asia, considering CWT approach as a controlling factor for future climate change scenarios. CWT representatives were dynamically downscaled with the RCM COSMO-CLM4.8 forcing ERA-40 reanalysis for historical simulation coupled with the future scenarios of the ECHAM5/MPI-OM1 models, the authors projected the changes in precipitation climatology over the Aksu basin until 2100. Outputs of statistical-dynamical approach show a decrease in annual precipitation over large parts of the Aksu river basin in Tien Shan Mountains and an opposite sign is defined to the southeast of the investigation area.

In contrast, many studies have investigated the large scale atmospheric circulation as a main driver of precipitation extremes by employing the weather typing approach using CMIP5 models for the last few years for Europe and other continents ([Santos et al., 2016](#); [El](#)

[Kenawy and McCabe, 2016](#); [Brigode et al., 2018](#)). All studies suggest that projected changes in large scale circulation can be robust indicators to investigate not only the precipitation climatology, but it would be beneficial for a wide range of climate change impact assessments and predictions of extreme events such as frequency and intensity of flooding and droughts, water resources and agricultural production under the global warming trends. The results of these studies provide inspiration to postulate that extreme rainy atmospheric circulation type can be a good indicator for mudflow frequency and intensity for the future in Uzbekistan.

Precipitation plays a major role in landslide formation, including mudslides, worldwide and the projected atmospheric circulation modulating precipitation extremes could predict such phenomena and help set up warning systems. A number of studies attempted to investigate the impact of global warming on different types of landslide occurrences by application of downscaled precipitation patterns as an input parameter obtained from GCMs ([Schmidt and Dehn, 2000](#); [Chiang and Chang, 2011](#)) and RCMs ([Schmidt and Glade, 2003](#)). These studies mainly focused on mountain and hilly areas prone to slope failures with the interaction of the climatic variables such as extreme rainfall events. The main drawback in the use of downscaled climate variables such as precipitation from GCMs output for landslide-climate analyses lie in the inherent uncertainty of downscaled climate projections ([Gariano and Guzzetti, 2016](#)). Additionally, raw GCM precipitation simulations may still have biases especially in the mountain regions ([Fowler et al., 2007](#); [Fang et al., 2015](#)). [Mannig et al. \(2013\)](#) suggested that additional model run would be desirable to assess the uncertainties and biases in the precipitation patterns in their study domain such as Central Asia. The authors suggested adoption of dynamical or statistical downscaling approaches to obtain high spatial and temporal resolution in order to examine climate change impacts on precipitation parameters. Inadequate observational or empirical data due to lack of meteorological stations in the study area has been often cited as a limitation (e.g. [Ozturk et al. \(2017\)](#) and [Reyers et al. \(2013\)](#)) to explain the model bias over the mountains and high plateau regions of Central Asia.

Mudflow rheology, dynamics and various other hydrogeological characteristics of natural hazard in Uzbekistan were carried out by many researchers ([Trofimov, 2006](#); [Chub et al., 2007](#); [Karpov and Pushkarenko, 1968](#); [Karpov et al., 1976](#); [Babko, 1978](#); [Isakova et al., 2009](#); [Juliev et al., 2019](#)). Climatologists such as [Salikhova \(1975\)](#) and [Lyakhovskaya \(1989\)](#) predicted mudflow occurrences in river basins and mountain areas of Uzbekistan based on analysis of synoptic circulation and remote sensing data. Unfortunately, the scarcity of studies on extreme weather events particularly landslides including mudflow occurrences in a changing climate in Uzbekistan is especially pronounced. Furthermore, the post-Soviet era scientific vacuum ([Xenarios et al., 2018](#)) created in Uzbekistan, similar to many post-Soviet countries still exists. To the best of our knowledge, mudflow occurrences in Uzbekistan under climate change conditions were investigated by [Chub \(2007\)](#) which was based on IPCC SRES scenarios (A2 and B2) indicating the risk initiated by rainfall will be increasing up to 50% by 2080. Moreover, third UNFCCC³ national report of Uzbekistan have also confirmed the increase of precipitation induced natural hazards such as mudflows to be 4 times more in the country by 2080.

[Gariano and Guzzetti \(2016, 2021\)](#) systematically documented the existing investigations world-wide; they detailed the concepts used in the selected studies and associated methodologies and included the results of analyses due to the climate change impact on different types of landslides. Geographical distribution of the climate change studies in relation to all type of landslide events for each country reported by [Gariano and Guzzetti \(2016, 2021\)](#) confirms that no peer-reviewed research regarding landslide (in our case mudflow) – climate change

³ https://unfccc.int/sites/default/files/resource/TNC_of_Uzbekistan_under_UNFCCC_english_n.pdf.

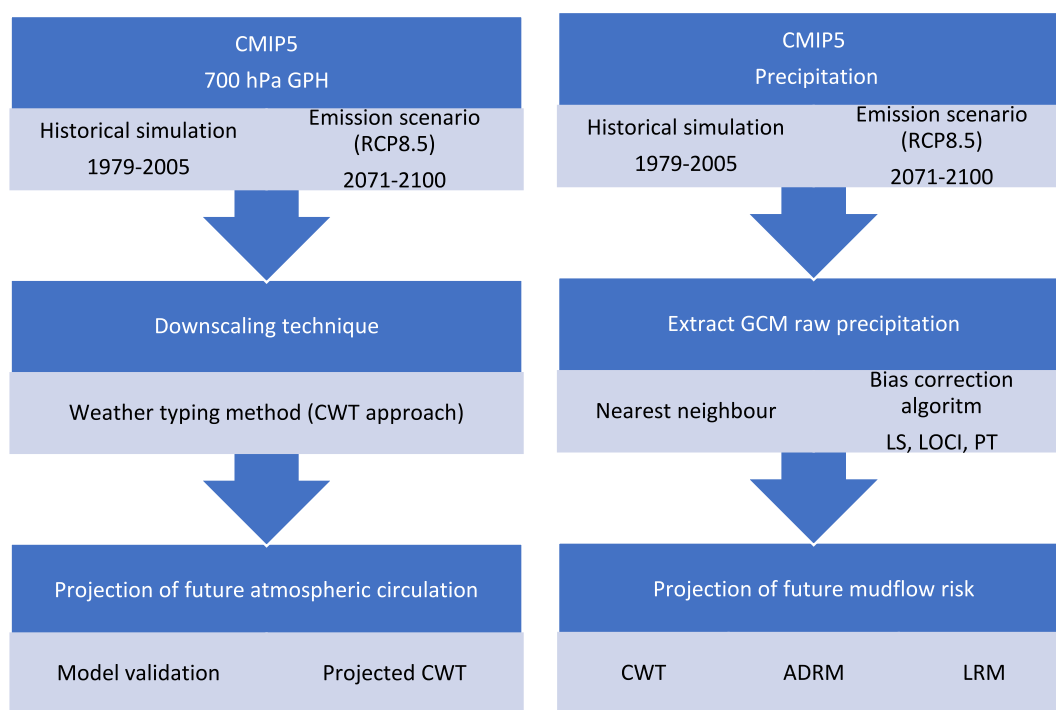


Fig. 1. Schematic flow chart of the methodology used in this study.

has been done in Central Asian countries including Uzbekistan. Therefore, the work presented in this research is one of the pioneer investigations analysing the potential impacts of future climate conditions in Uzbekistan, particularly, as a response to changes in large scale atmospheric circulation as a main driver of precipitation extremes induced mudflows in the piedmont and mountainous areas of the country.

Considering the climate change studies on atmospheric circulation and projections for precipitation induced extreme landslide events across the globe, the main scope and aims of this study are twofold: 1) to construct recent and future changes of large scale atmospheric circulation defined on a daily basis as a diagnostic tool for a more comprehensive dynamical interpretation of precipitation driving mechanisms and its association with mudflow frequencies in Uzbekistan, 2) to evaluate the skills of CMIP5 models to replicate precipitation threshold known to trigger potential mudflow occurrences under both current and future idealised climates over the study area, and 3) to use this knowledge to further assess the mechanisms inducing mudflows associated with extreme precipitation in a longer time scale over Uzbekistan.

2. Data

2.1. Reanalysis of geopotential height field

The ERA-Interim global atmospheric reanalysis data (Dee et al., 2011) is applied as a reference for the 27-year historical period 1979–2005. Only daily mean geopotential height field at 700 hPa (Z_{700} hereafter) is considered in this study. The gridded data set has 0.75° spatial resolution (approximately 80 km) and 12 h temporal resolution. Reanalysis data is available at ECMWF's meteorological archive.⁴

2.2. CMIP5 GCM outputs

The daily mean Z_{700} outputs from 10 GCMs namely ACCESS1-0, bcc-csm1-1, CMCC-CM, CNRM-CM5, GFDL-CM3, HadGEM2-CC, HadGEM2-

ES, IPSL-CM5A-LR, MIROC5 and MPI-ESM-LR of the CMIP5 (Taylor et al., 2012) projection are considered in this study. The atmospheric component of horizontal and vertical resolutions for each model and other main characteristics of each GCM are described in Table A1.

The daily outputs of two different experiments are applied:

1. The “historical” experiment or a simulation of the recent past under the historical forcing which is available for the years 1950–2005.
2. The Representative Concentration Pathways “RCP8.5” scenario or the high radiative forcing surplus at approximately 8.5 W/m² available from 2006 to 2100.

For all models and experiments, only the first ensemble member (r1i1p1) is considered. The time period for historical simulations evaluated in this study is 1979–2005 and for the future scenario is 2071–2100.

Shortlisted 10 GCMs (ACCESS1-0, bcc-csm1-1, CMCC-CM, CNRM-CM5, GFDL-CM3, HadGEM2-CC, HadGEM2-ES, IPSL-CM5A-LR, MIROC5 and MPI-ESM-LR) from the multimodel CMIP5 ensemble (Table A1) for historical run (1979–2005) and future scenarios (2071–2100) of precipitation are also used in this study. The main focus is precipitation timeseries for the warm season of the year (March–August) since all recorded mudflow episodes with different origins mostly occur during this period and it is towards to examine the long-term impact of climate change on precipitation threshold resulting mudflows over the study area. CMIP5 data used in this paper is available on CEDA⁵ and CERA⁶ online archives.

2.3. Observed data

Daily observed precipitation data for a period of 27 years (1979–2005) from the Gallyaaraal and Sokh stations (Fig. 2) recorded by Uzhydromet according to WMO standards is used for bias correction of

⁴ <https://apps.ecmwf.int/datasets/data/interim-full-daily/levtype=sfc/>.

⁵ <http://data.ceda.ac.uk/badc/cmip5/data/cmip5/output1/>.

⁶ <https://cera-www.dkrz.de/WDCC/ui/cersearch/>.

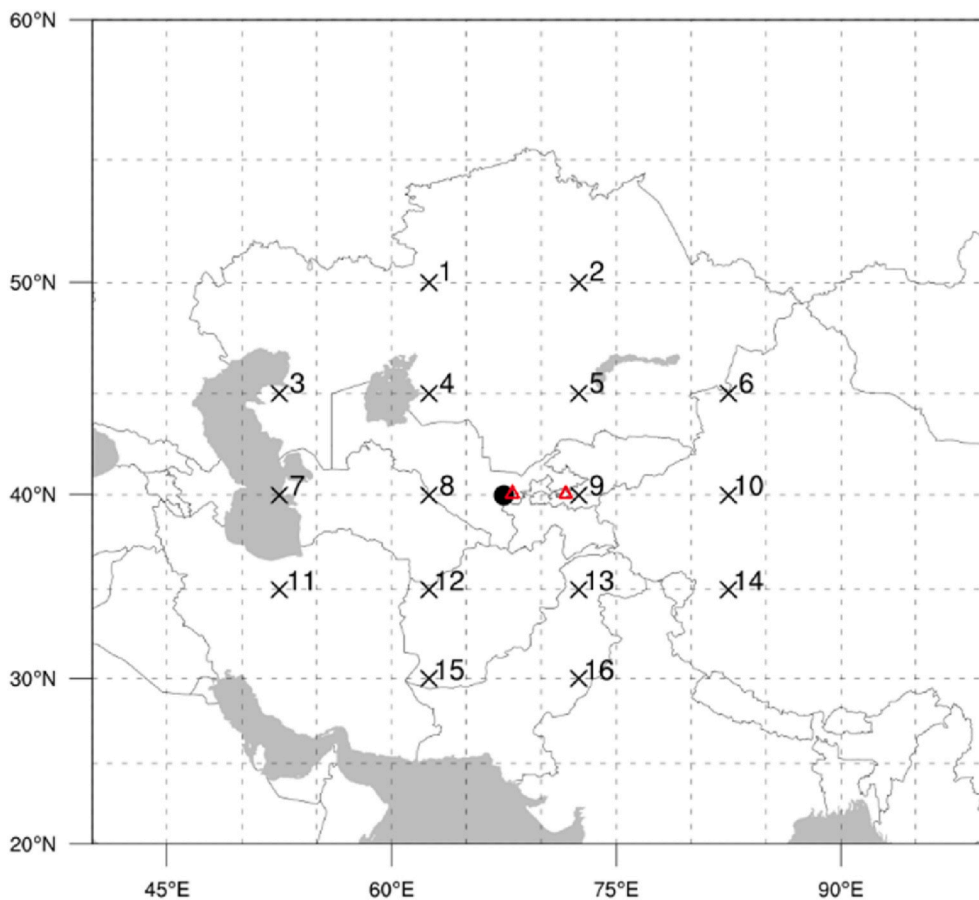


Fig. 2. Location of the grid points over Uzbekistan and Central Asia used in the calculation of the CWT. The allocated grid point numbers are used in the equations given in Jones et al. (1993). Black dot is the central grid point (40.0°N-67.5°E) used in this study. The pressure value of the central grid point is not considered in the equation. Representative stations Gallyaaraal (40.02°N-67.60°E) and Sokh (39.97°N-71.13°E) are indicated in red triangles. (For interpretation of the references to colour in this figure legend, the reader is referred to the Web version of this article.)

GCM predictors and validation of the historical experiment.

3. Methods

Fig. 1 presents the systematic approach implemented in this research. First, 10 CMIP5 models namely ACCESS1-0, bcc-csm1-1, CMCC-CM, CNRM-CM5, GFDL-CM3, HadGEM2-CC, HadGEM2-ES, IPSL-CM5A-LR, MIROC5 and MPI-ESM-LR have been shortlisted based on data availability and data quality at all pressure levels over the entire investigation area for a predictor used in this paper. Evaluation of 10 GCMs from CMIP5 projection was conducted to examine the effects of anthropogenic climate change on large scale atmospheric circulation by adopting statistical downscaling approach namely circulation weather type (CWT) for the recent (1979–2005) and future (2071–2100) climates in Uzbekistan. In the next step, GCM outputs were applied to an empirical-statistical antecedent daily rainfall model (ADRM) to assess the effect of anthropogenic emissions of greenhouse gases on precipitation threshold inducing mudflows for the target period of 2071–2100 in the study area. For this purpose, the extracted daily precipitation timeseries from the CMIP5 GCMs for the control run (1979–2005) and future experiment (2071–2100) under the RCP8.5 emission scenario was examined by bias correction procedure. Then, the CMIP5 GCMs were evaluated by calculating frequency means between the station-based climate and the raw precipitation by CMIP5 and bias corrected values. The results of two selected GCMs out of 10 were used to run the ADRM together with logistic regression model (LRM). The analysis demonstrates that model outputs for climate change studies are capable to predict mudflow occurrences and is unique to this field of research for Uzbekistan.

3.1. CWT classification of the historical and future experiments

CWT approach is used as perfect prognosis statistical downscaling method (Maraun and Widmann, 2018) to link the large scale predictors (circulation type in this case) to local scale predictands (precipitation and mudflow occurrences).

Before the downscaling process, the daily mean Z_{700} historical and future experiments data from 10 GCMs of CMIP5 multi-model projection are interpolated using bilinear interpolation onto the same horizontal resolution as the ERA-Interim reanalysis (0.75° longitude × 0.75° latitude) using Climate Data Operator (CDO) application. Therefore, CMIP5 GCM outputs are statistically downscaled to define the frequency of each weather type by CWT approach (Jones et al., 1993) which is initially based on the Lamb weather types scheme for the British Isles (Lamb, 1972).

Using calculations of total shear vorticity (Z), the resultant flow strength (F), and direction (with an increment of 45°), the Lamb scheme can provide information on the pure airflow direction (northerly, southerly, easterly, westerly, north-easterly, north-westerly, south-easterly and south-westerly, corresponding to N, S, E, W, NE, NW, SE, and SW), non-direction type (i.e., cyclonic, anticyclonic) of the flow, hybrid types (CN, CS, CE, CW, CNE, CNW, CSE, CSW, AN, AS, AE, AW, ANE, ANW, ASE, and ASW) and undefined class (U). The southerly flow (SF), westerly flow (WF), total flow (F), southerly shear vorticity (ZS), and westerly shear vorticity (ZW) are computed from pressure at Z_{700} level at the 16 grid points (1–16) shown in Fig. 2 using the following formulas:

$$W = \frac{1}{2}(12 + 13) - \frac{1}{2}(4 + 5) \quad (1)$$

Table 1
Circulation types defined by total shear vorticity (Z) and resultant flow (F).

Weather type acronym	Calculation
Directional (N, NE, E, SE, S, SW, W, NW)	$ Z < F$
Cyclonic (C)	$ Z > 2F, Z > 0$
Anticyclonic (A)	$ Z > 2F, Z < 0$
Unclassified cyclonic (UC)	$Z < \text{mean annual } Z, F < \text{mean annual } F, Z > 0$
Unclassified anticyclonic (UA)	$Z < \text{mean annual } Z, F < \text{mean annual } F, Z < 0$
Cyclonic hybrid (HYC)	$F < Z < 2F \text{ and } Z > 0$
Anticyclonic hybrid (HYA)	$F < Z < 2F \text{ and } Z < 0$

$$S = 1.74 \left[\frac{1}{4}(5 + 2 \times 9 + 13) - \frac{1}{4}(4 + 2 \times 8 + 12) \right] \quad (2)$$

$$F = (S^2 + W^2)^{1/2} \quad (3)$$

$$ZW = -1.07 \left[\frac{1}{2}(15 + 16) - \frac{1}{2}(8 + 9) \right] - 0.95 \left[\frac{1}{2}(8 + 9) - \frac{1}{2}(1 + 2) \right] \quad (4)$$

$$ZS = 1.52 \left[\frac{1}{4}(6 + 2) \times 10 + 14 \right] - \frac{1}{4}(5 + 2 \times 9 + 13) - \frac{1}{4}(4 + 2 \times 8 + 12) + \frac{1}{4}(3 + 2 \times 7 + 11) \quad (5)$$

$$Z = ZW + ZS \quad (6)$$

The following rules (Table 1) need to be taken into account in order to define the appropriate weather circulation based on Lamb classification scheme.

In this study similar to Mamadjanova et al. (2018), the CWT objective method generates a daily circulation database based on ERA-Interim reanalysis (1979–2005) and 10 GCMs from CMIP5 projection for historical run (1979–2005) and future scenario (2071–2100) of 11 basic groups which include eight directional, two synoptic and unclassified types (AC, C, N, NE, E, SE, S, SW, W, NW, undefined) around a central point located (40.0°N-67.5E°) over Uzbekistan (Fig. 2 and A1).

3.1.1. Bias and climate change signal

CWT seasonal frequencies of historical experiments from CMIP5 GCMs are substantially biased compared to real climate data (ERA-Interim reanalysis in this case). This is calculated by the following equation (7) adopted from Maraun and Widmann (2018):

$$Bias_{\theta}(Z_{700}) = \theta_{mod}(Z_{700}) - \theta_{obs}(Z_{700}) \quad (7)$$

where, $Bias_{\theta}(Z_{700})$ is a systematic difference between a historical simulation of GCMs $\theta_{mod}(Z_{700})$ for the period of 1979–2005 and an observed data $\theta_{obs}(Z_{700})$ for the same period as a model data.

The CWT projection for the 10 CMIP5 GCMs ensemble scenarios constructed as a seasonal rate per CWT class attributable to climate change signal calculated by formula (8):

$$A_{CWT}(Z_{700}) = CWT_{sce}(Z_{700}) - CWT_{pres}(Z_{700}) \quad (8)$$

where, $A_{CWT}(Z_{700})$ is burden of CWT frequency attributable to climate change, CWT is a frequency per airflow direction, $CWT_{sce}(Z_{700})$ is the CWT frequency for the years 2071–2100, $CWT_{pres}(Z_{700})$ CWT frequency for the present time period 1979–2005.

3.2. Extraction of CMIP5 ensemble daily rainfall timeseries

Before the extraction CMIP5 GCMs precipitation data, selected 10 models were interpolated using bilinear algorithm. Thereafter, the grid

box that included the location of selected weather stations Gallyaarl and Sokh (Fig. 2) used to extract raw precipitation values from CMIP5 GCMs based on nearest grid point interpolation using CDO commands. Daily rainfall values for the 10 selected GCMs for historical simulation (1979–2005) were extracted in order to validate the raw data with the observational timeseries. Daily rainfall values for future scenario 2071–2100 under the RCP8.5 emission were also extracted at the same grid box.

3.3. Bias correction methods for GCM precipitation data

The choice of a bias correction algorithm plays a significant role in assessing the precipitation pattern for recent and future climate conditions. In this study, three bias correction methods such as linear scaling (LS), local intensity scaling (LOCI) and power transformation (PT) are employed for adjusting GCMs outputs. Timeseries of daily precipitation data for the period of 1979–2005 and 2071–2100 are used for bias correction techniques.

3.3.1. Linear scaling of precipitation

The linear scaling (LS) or simply scaling method introduced by Lenderink et al. (2007) quantifies the bias by application of monthly correction values based on the differences between observed and raw data of the model (Fang et al., 2015). The formula for LS is:

$$P_{cor,m,d} = P_{raw,m,d} \times \frac{\mu(P_{obs,m})}{\mu(P_{raw,m})} \quad (9)$$

$P_{cor,m,d}$ is corrected precipitation on the d th day of m th month, and $P_{raw,m,d}$ is the model raw precipitation on the d th day of m th month. μ represents the expectation operator (e.g., $\mu(P_{obs,m})$ represents the mean value of observed precipitation at given month m).

3.3.2. Local intensity scaling of precipitation

Local intensity scaling method (LOCI) presented by Schmidli et al. (2006) consists of three steps (Teutschbein and Seibert, 2012) that can effectively correct for biases during the wet-day frequency and intensity. In a first step, a model precipitation threshold for the m th month ($P_{thres,m}$) is calibrated such that the number of GCM simulated days exceeding this threshold matches the number of observed days with precipitation more than 0 mm (Teutschbein and Seibert, 2012; Fang et al., 2015). Thereafter, the following formula quantifies a scaling factor s from the wet day intensities:

$$s_m = \frac{\mu(P_{obs,m,d} | P_{obs,m,d} > 0)}{\mu(P_{raw,m,d} | P_{raw,m,d} > P_{thres,m})} \quad (10)$$

Finally, GCM simulated precipitation is corrected by the scale parameter:

$$P_{cor,m,d} = \begin{cases} 0, & \text{if } P_{raw,m,d} < P_{thres,m} \\ P_{raw,m,d} \times s_m & \text{if } P_{raw,m,d} > P_{thres,m} \end{cases} \quad (11)$$

3.3.3. Power transformation of precipitation

The power transformation (PT) approach uses an exponential form to further adjust the variance statistics of precipitation time series while the above two algorithms (LS and LOCI) are limited to correct the differences in the variance (Teutschbein and Seibert, 2012). Following Fang et al. (2015) b_m the exponent for the m th month is estimated (Shrestha, 2015) by the LOCI combination approach formula:

$$f(b_m) = \frac{\sigma(P_{obs,m})}{\mu(P_{obs,m})} - \frac{\sigma(P_{LOCI,m}^{b_m})}{\mu(P_{LOCI,m}^{b_m})} \quad (12)$$

where σ indicates the standard deviation, $P_{LOCI,m}$ is the corrected precipitation by the LOCI algorithm for the m th month. If the exponent

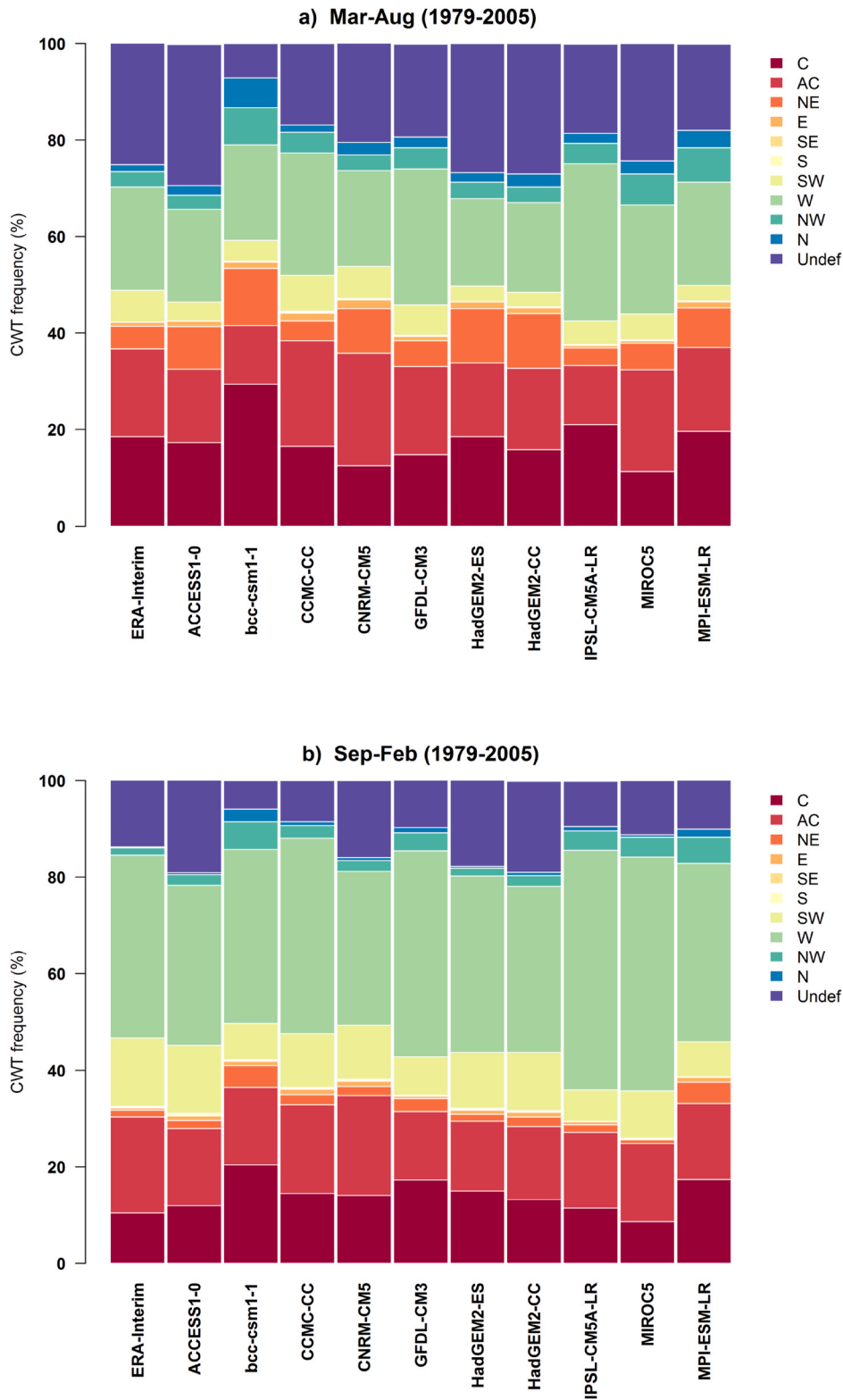


Fig. 3. Seasonal frequencies of ERA-Interim reanalysis and 10 CMIP5 GCMs historical experiments for each CWT for the period of 1979–2005.

factor b is greater than 1 for the m th month it means that the GCMs underestimates the coefficient of variances of observed precipitation timeseries for the m th month. After the identification of the b_m factor, the parameter

$$s_m = \frac{\mu(P_{obs,m})}{\mu(P_{LOCI,m}^{b_m})} \tag{13}$$

is adjusted in a stepwise manner to match the mean corrected values to the observed mean. Thereafter, the corrected precipitation timeseries by LOCI approach is used:

$$P_{cor,m,d} = s_m \times P_{LOCI,m,d}^{b_m} \tag{14}$$

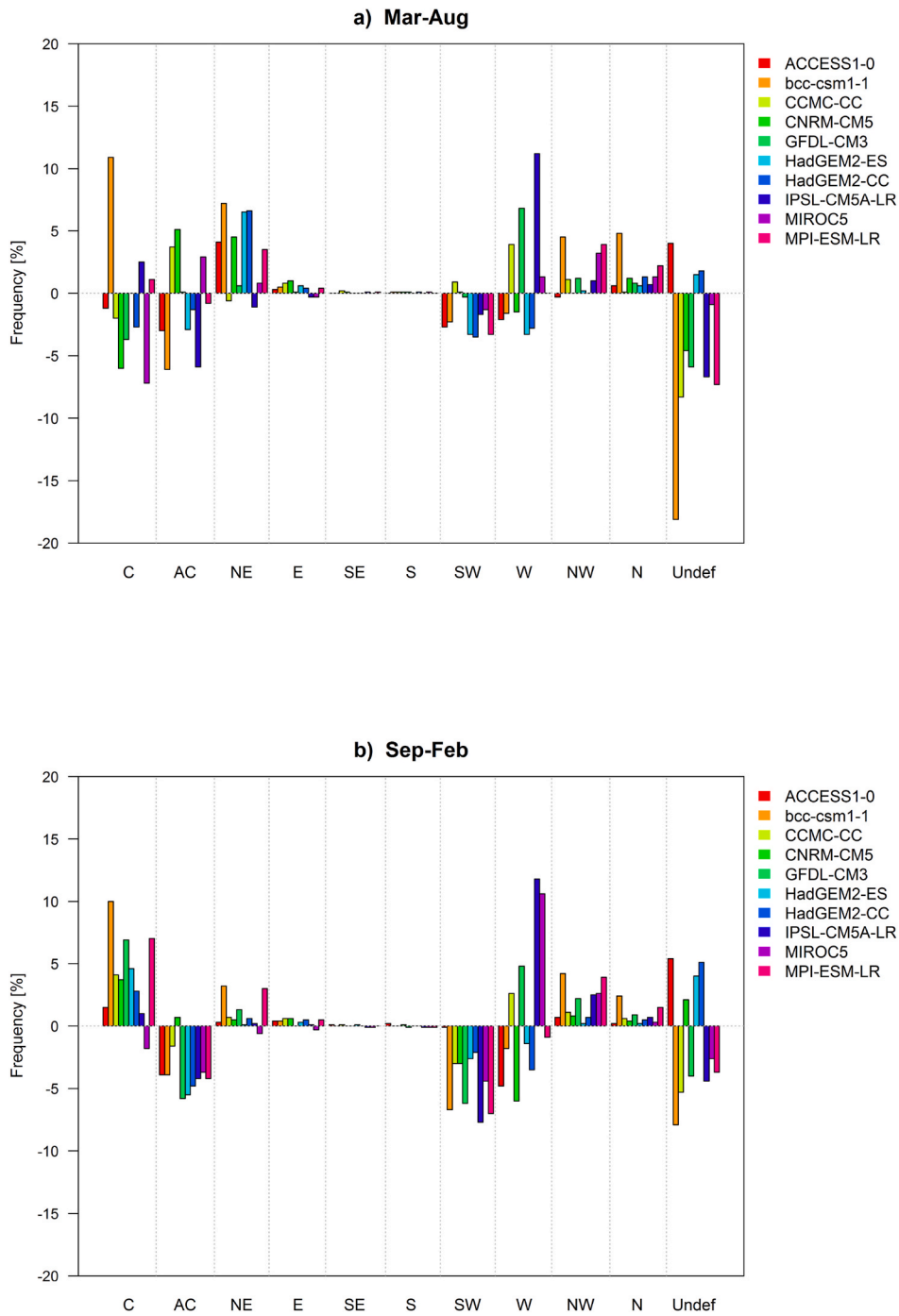


Fig. 4. Seasonal differences between historical experiments in 10 CMIP5 models and ERA-Interim reanalysis (1979–2005 GCM minus 1979–2005 ERA-Int) over Uzbekistan at 700 hPa GPH.

3.4. Antecedent daily rainfall method

The antecedent daily rainfall model (ADRM) introduced by Crozier and Eyles (1980) is based on simple formula:

$$ra_0 = kr_1 + k^2r_2 + \dots + k^n r_n \tag{15}$$

where ra_0 is the antecedent daily rainfall for day 0; r_1 is the rainfall on the day before day 0; r_n is the rainfall on the n th day before day 0; and k is a constant < 1.0 , in this case $k = 0.84$.

After the calculation of antecedent rainfall index of bias corrected precipitation from two GCMs (CMCC-CM and MPI-ESM-LR) obtained by PT approach, the daily rainfall value as a driving factor of mudflow

occurrences in the study area is applied to ADRM for the control run and future scenario.

3.5. Logistic regression model

Logistic regression (LRM) is based on the idea transforming the predict and (mudflow in this case) to a binary (or dummy variable), taking in the values zero and one (Hosmer and Lemeshow, 2000; Wilks, 2011) expressed in equation (16):

$$x_2 = \begin{cases} 1, & \text{if } x_1 > c \\ 0, & \text{if } x_2 \leq c \end{cases} \tag{16}$$

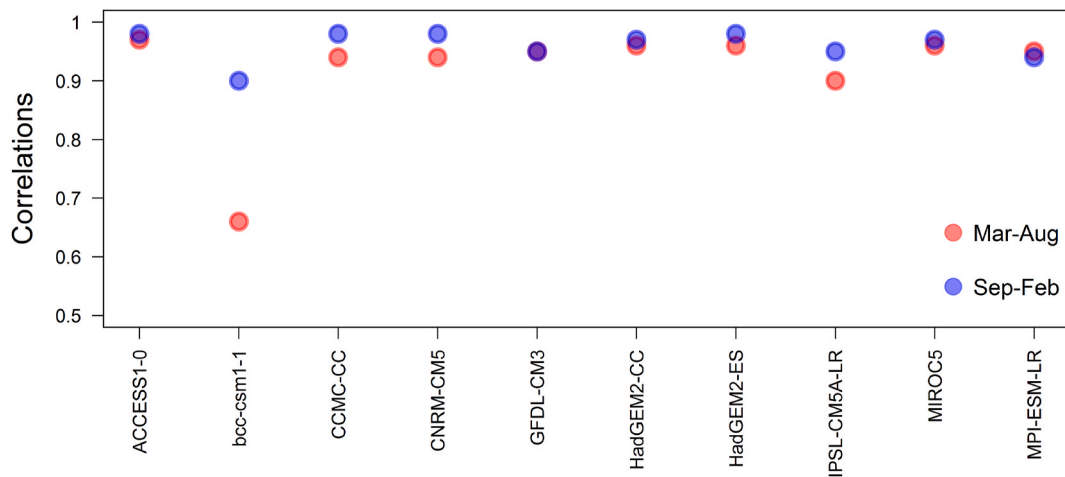


Fig. 5. Pearson correlations between CWT frequencies of ERA-Interim and 10 GCMs historical experiences of CMIP5 projection over the study area for the March–August (red circle) and September–February (blue) of 1979–2005 years. (For interpretation of the references to colour in this figure legend, the reader is referred to the Web version of this article.)

where x_2 is a binary variable (mudflow occurrence), x_1 predictor (daily precipitation and daily antecedent rainfall index), 1 is presence of mudflows and 0 can be assigned if no mudflow is present.

LRM technique is fit to binary predictands using log-odds, or *logit*, link function $g(p) = \ln\left[\frac{p}{1-p}\right]$, yielding the generalised linear function is expressed in the formulation of 17.

$$\ln\left(\frac{p_i}{1-p_i}\right) = b_0 + b_1x_1 + \dots + b_kx_k \quad (17)$$

where p_i is predicted value from the i th set of predictors, b is slope or gradient, x is predictor variable, K is single predictor case, when $b_0 + b_1x_1 \rightarrow +\infty$ exponential function approach becoming large than the predicted value p_i , in case $b_0 + b_1x_1 \rightarrow -\infty$ the p_i approaches zero.

The values of the variables are the input data for the logistic algorithm to calculate the precipitation threshold equation and plot probability (P) curves for $P = 0.1$, $P = 0.5$ and $P = 0.9$. This approach is analogous to the one presented in Glade et al. (2000).

3.6. Selection of extreme rainfall events triggering mudflows

Based on results in Mamadjanova et al. (2018), the precipitation values for more than 20 mm and antecedent index with ≤ 40 mm during the CWT C, SW and W days have been derived from the bias corrected precipitation data for control run (1979–2005) and future projection (2071–2100) simulated for the Gallyaaraal station. It was assumed that the chance of mudflow occurrences in case of precipitation below 20 mm is relatively less, and this assumption has been validated in Mamadjanova et al. (2018) whereby it shows that there is only 10% probability of mudflow occurrences for the Gallyaaraal area when precipitation amount is ≤ 20 mm. However, it should be duly taken into account that higher antecedent rainfall index could trigger mudflow magnitude even though the precipitation amount is less than 20 mm. The limitation of this approach lies with the fact that only daily rainfall values are included as mudflow inducing factor and neglecting temperature patterns.

4. Results

4.1. Changes in CWT frequencies experimented by CMIP5 GCMs

4.1.1. Historical experiments of seasonal CWT

The effects of large-scale atmospheric circulation over Uzbekistan have been examined by evaluating GCMs ensemble to simulate the

historical CWT frequencies for the warm and cold periods of 1979–2005. The seasonal frequencies of CWT are generally well simulated by applying statistical downscaling procedure. Fig. 3 presents ERA-Interim outputs and historical experiments of seasonal distribution for each weather type simulated by 10 CMIP5 GCMs. Based on the findings of the statistical downscaling, compared to the observational data (ERA-Interim in this case) most models capture the seasonal frequencies of CWT as same as in observation or with small discrepancies.

Fig. 4 summarizes the frequency changes calculated between ERA-Interim and GCM historical experiment for the period of 1979–2005. From the 10 GCMs ACCESS1-0, HadGEM2-ES, HadGEM2-CC and MPI-ESM-LR represent nearly realistic outputs of CWT frequencies for the historical period with less than 5% of changes for each CWTs for the warm and cold periods of the year. Only NE flow (6.5%) in March–August is overestimated by both HadGEM2 models also C days (7%) in September–February is increased by MPI-ESM-LR.

In contrast, bcc-csm1-1 model performs the CWT frequency differences significantly throughout the year. This model overestimates (10–12%) the frequency of cyclonic days and underestimates (8–18%) the undefined circulation type over the historical period. Therefore, this model overestimates the NE airflow (7.2%) in summer and SW flow (6.7%) in winter period of the year.

The CCMC-CC model simulates well and underestimates slightly only the days of undefined flow direction in March–August (7%) and September–February (5.3%). Further remarkable results between observation and biases achieved by simulation of CNRM-CM5 with minor decreases on C days in summer (6%) and W flow in winter (6%).

GFDL-CM3 overestimates slightly the W days (6.8%) in winter and C days (6.9%) in summer, as well as underestimates AC (5.8%) and SW (6.2%) airflow directions in winter. This model also is similar to most of the models and reproduces the decrease of undefined weather type (5.9%) especially in the warm phase of the year. However, IPSL-CM5A-LR underestimates AC (5.9%), undefined weather type (6.7%) in summer and overestimates W airflow during the warm (11.2%) and cold (11.8%) phases of the year. The frequency of C days (7.2%) in a warm period is underestimated and W days (10.6%) in cold phase of the year is overestimated by MIROC5.

The correlation distributions of the CWT frequencies of each GCM for the warm and cold periods of the year show that historical experiments of selected models match well with the observation (Fig. 5). However, bcc-csm1-1 differs from the other models and observation and significantly maintains CWT changes and uncertainties, especially in warm season of the year. Therefore, it is reasonable that historical simulation of CWT frequencies of selected models can reproduce accurately, to a

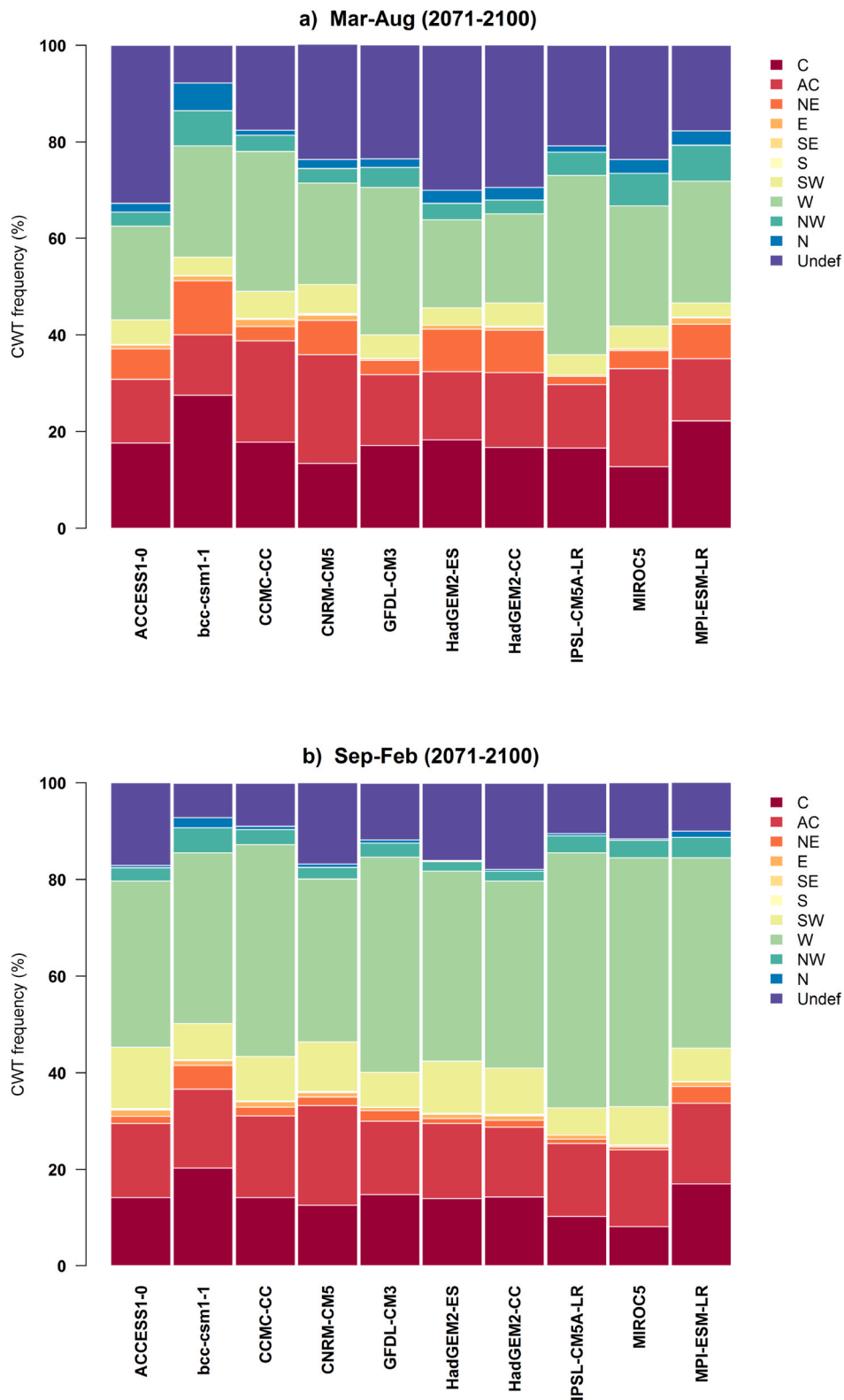


Fig. 6. Scenario of seasonal frequencies of CWT under the selected 10 GCMs for the period of 2071–2100.

great extent, the large-scale atmospheric circulation over Uzbekistan and CA.

4.1.2. Future projections of CWT frequencies

The effects of changes in large scale atmospheric circulation frequencies over Uzbekistan and Central Asia at the end of this century

2100, under RCP8.5 scenario (Fig. 6) is explored in this section. Fig. 7 and Tables 2–3 display the changes in the CWT frequencies in lower troposphere (Z_{700}) over the study area (2071–2100 minus 1979–2005).

The results of CMIP5 GCMs suggest that CWT W direction will become more frequent and increase up to 4.5% in the target period of 2071–2100. Of the 10 GCMs selected, only the bcc-csm1-1 model shows

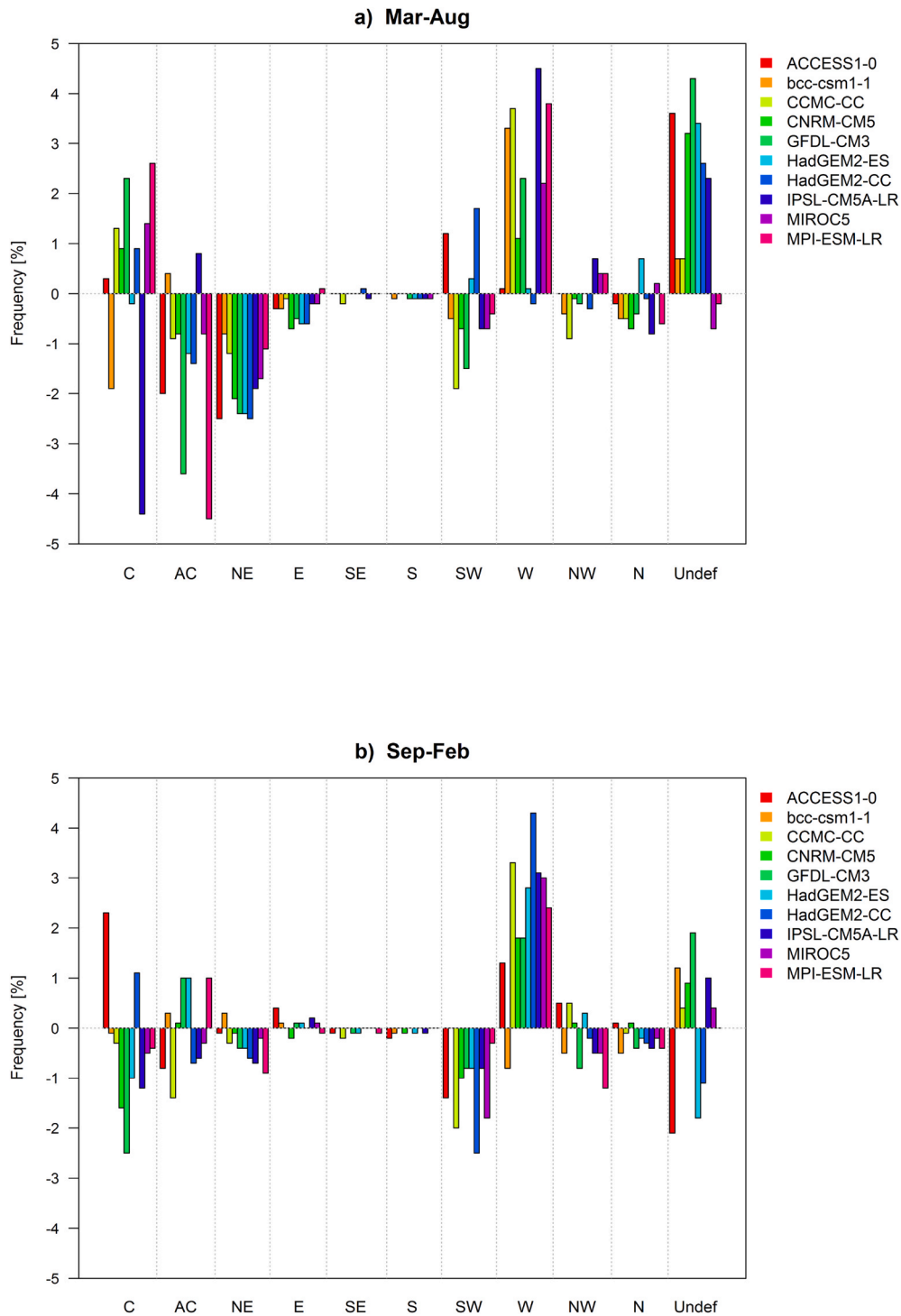


Fig. 7. Seasonal frequencies of CWT for CMIP5 GCMs scenarios (2071–2100 minus 1979–2005) over Uzbekistan at 700 hPa GPH.

that W airflow will decrease (−0.8%) during the period of September–February in the future.

7 GCMs of the 10 diagnose that the CWT C weather will be actively increasing in the warm season up to 2.6%. The bcc-csm1-1 model and IPSL-CM5A-LR show that cyclonic days will be less frequent in summer (−1.9% and −4.4%). In contrast to the warm period, the cyclonic circulation will be less active during the cold season (September–February) in the future; only ACCESS1-0 and HadGEM2-CC models highlight that C days will be stronger by increasing its frequency up to 2.3% in the winter for the 2071–2100 period.

CWT AC days will decrease up to −4.5% in the warm phase,

however, there are model uncertainties for the cold period of the year. In contrast to the CWT AC days, the CWT SW airflow will decrease in cold season of the year and there are model uncertainties during the warm season in the future. The three models, ACCESS1-0, HadGEM2-ES and HadGEM2-CC show increase (from +0.3% to +1.7%), whereas the remaining seven models show decrease (from −0.4% to −1.9%) in the SW circulation lower troposphere during the summer for the 2071–2100 period.

The projections of the ensemble of CMIP5 models show that NE and N atmospheric circulations will decrease, especially the NE type show a decrease of up to −2.5% (March–August) over the study area in the

Table 2

Climate change signal for the warm season of March–April (2071–2100 minus 1979–2005) in the CWT frequencies (%) in each weather class and for each model (for the expansions of model abbreviation and acronym see [Table A1](#)).

Model name	Circulation Weather Type (CWT)										
	C	AC	NE	E	SE	S	SW	W	NW	N	Und
ACCESS1-0	0.3	-2	-2.5	-0.3	0	0	1.2	0.1	0	-0.2	3.6
bcc-csm1-1	-1.9	0.4	-0.8	-0.3	0	-0.1	-0.5	3.3	-0.4	-0.5	0.7
CMCC-CM	1.3	-0.9	-1.2	-0.1	-0.2	0	-1.9	3.7	-0.9	-0.5	0.7
CNRM-CM5	0.9	-0.8	-2.1	-0.7	0	0	-0.7	1.1	-0.1	-0.7	3.2
GFDL-CM3	2.3	-3.6	-2.4	-0.5	0	-0.1	-1.5	2.3	-0.2	-0.4	4.3
HadGEM2-CC	0.9	-1.4	-2.5	-0.6	0.1	-0.1	1.7	-0.2	-0.3	-0.1	2.6
HadGEM2-ES	-0.2	-1.2	-2.4	-0.6	0	-0.1	0.3	0.1	0	0.7	3.4
IPSL-CM5A-LR	-4.4	0.8	-1.9	-0.2	-0.1	-0.1	-0.7	4.5	0.7	-0.8	2.3
MIROC5	1.4	-0.8	-1.7	-0.2	0	-0.1	-0.7	2.2	0.4	0.2	-0.7
MPI-ESM-LR	2.6	-4.5	-1.1	0.1	0	0	-0.4	3.8	0.4	-0.6	-0.2
Ensemble mean	0.3	-1.4	-1.9	-0.3	-0.02	-0.1	-0.3	2.1	-0.04	-0.3	2

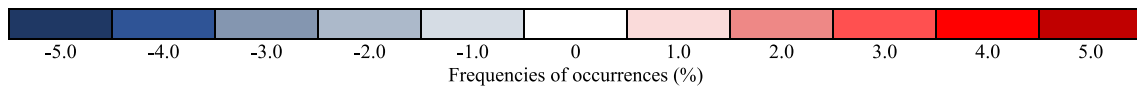
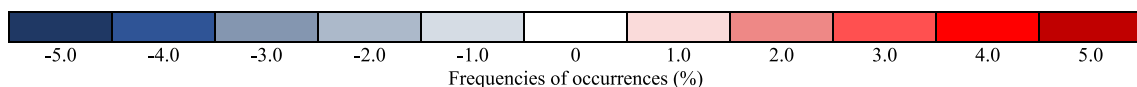


Table 3

Same as [Table 2](#) but for the period of September–February (2071–2100 minus 1979–2005).

Model name	Circulation Weather Type (CWT)										
	C	AC	NE	E	SE	S	SW	W	NW	N	Und
ACCESS1-0	2.3	-0.8	-0.1	0.4	-0.1	-0.2	-1.4	1.3	0.5	0.1	-2.1
bcc-csm1-1	-0.1	0.3	0.3	0.1	0	-0.1	0	-0.8	-0.5	-0.5	1.2
CMCC-CM	-0.3	-1.4	-0.3	0	-0.2	0	-2	3.3	0.5	-0.1	0.4
CNRM-CM5	-1.6	0.1	-0.1	-0.2	0	-0.1	-1	1.8	0.1	0.1	0.9
GFDL-CM3	-2.5	1	-0.4	0.1	-0.1	0	-0.8	1.8	-0.8	-0.4	1.9
HadGEM2-CC	1.1	-0.7	-0.6	0	0	0	-2.5	4.3	-0.2	-0.3	-1.1
HadGEM2-ES	-1	1	-0.4	0.1	-0.1	-0.1	-0.8	2.8	0.3	-0.2	-1.8
IPSL-CM5A-LR	-1.2	-0.6	-0.7	0.2	0	-0.1	-0.8	3.1	-0.5	-0.4	1
MIROC5	-0.5	-0.3	-0.2	0.1	0	0	-1.8	3	-0.5	-0.2	0.4
MPI-ESM-LR	-0.4	1	-0.9	-0.1	-0.1	0	-0.3	2.4	-1.2	-0.4	0
Ensemble mean	-0.4	-0.04	-0.3	0.1	-0.1	-0.1	-1.1	2.3	-0.2	-0.2	0.1



future. The CWT E, SE and S days will remain at the same level or change by $\pm 0.6\%$ in the 2071–2100 years. Model uncertainties exist for the CWT NW flow direction with the amount of $\pm 1\%$ in the future. Due to the topography, the undefined weather type is projected to increase (4.3%) notably in warm phase of the year.

In general, based on the CMIP5 GCMs ensemble results it can be predicted that CWT frequencies and magnitudes will not change in some cases (CWT SE and S), as ensemble mean has clear anomalous results with maximum seasonal variation $\pm 2.3\%$ in the diagnostic period of 2071–2100 ([Tables 2–3](#)). However, it can be concluded that CWT C and

Table 4

Frequency based statistics (unit: mm) of daily mean observed precipitation, GCM raw data and bias-corrected values (LS, LOCI, PT) at the Gallyaaraal station for the historical period (1979–2005) and future scenario (2071–2100).

		standard deviation		mean		median		75th percentile		99th percentile	
		control	scenario	control	scenario	control	scenario	control	scenario	control	scenario
ACCESS1-0	Obs	0.98		1.04		0.84		1.70		3.52	
	Raw	1.54	1.81	1.84	2.18	1.63	2.13	2.68	3.43	5.87	6.74
	LS	0.86	1.12	1.04	1.30	1.02	1.23	1.66	2.09	3.39	3.96
	LOCI	1.40	3.31	1.65	3.87	1.47	3.41	2.69	5.87	4.85	13.32
	PT	0.94	1.52	1.04	1.53	0.90	1.24	1.58	2.47	4.01	6.57
bcc-csm1-1	Obs	0.98		1.04		0.84		1.70		3.52	
	Raw	0.88	0.91	1.09	0.99	1.09	0.84	1.78	1.71	3.07	3.11
	LS	0.84	0.89	1.05	0.95	1.04	0.81	1.64	1.55	2.97	3.24
	LOCI	1.33	1.54	1.65	1.54	1.52	1.03	2.72	2.62	4.93	5.39
	PT	1.02	1.37	1.04	1.13	0.84	0.64	1.61	1.64	3.69	5.95
CMCC-CM	Obs	0.98		1.04		0.84		1.70		3.52	
	Raw	0.97	1.24	1.04	1.7	0.93	0.87	1.68	1.93	3.86	4.57
	LS	0.97	1.35	1.04	1.21	0.92	0.84	1.69	1.89	3.75	5.56
	LOCI	0.99	1.37	1.05	1.22	0.93	0.84	1.67	1.93	3.77	5.72
	PT	0.97	1.41	1.04	1.23	0.91	0.82	1.65	1.98	3.70	6.15
CNRM-CM5	Obs	0.98		1.04		0.84		1.70		3.52	
	Raw	1.19	1.28	1.34	1.42	1.21	1.11	2.09	2.27	4.60	4.74
	LS	0.95	1.08	1.04	1.13	0.91	0.86	1.70	1.78	3.60	4.22
	LOCI	1.08	1.19	1.25	1.31	1.13	1.05	1.89	2.04	4.23	4.49
	PT	1.00	1.18	1.04	1.16	0.85	0.80	1.70	1.79	3.71	4.42
GFDL-CM3	Obs	0.98		1.04		0.84		1.70		3.52	
	Raw	0.79	0.78	1.02	0.94	1.04	0.94	1.63	1.53	2.83	2.83
	LS	0.84	0.85	1.05	0.97	1.05	0.92	1.72	1.64	3.10	3.18
	LOCI	1.33	1.36	1.59	1.47	1.51	1.31	2.59	2.52	4.57	4.90
	PT	0.97	1.22	1.04	1.13	0.89	0.83	1.73	1.77	3.78	4.63
HadGEM2-CC	Obs	0.98		1.04		0.84		1.70		3.52	
	Raw	1.37	1.90	1.50	2.01	1.14	1.64	2.17	3.23	5.47	7.37
	LS	0.88	1.34	1.04	1.46	0.98	1.38	1.68	2.46	2.99	4.89
	LOCI	1.73	2.43	1.74	2.43	1.33	2.00	2.72	3.88	7.33	9.62
	PT	0.99	1.89	1.04	1.82	0.87	1.41	1.68	3.11	3.59	7.60
HadGEM2-ES	Obs	0.98		1.04		0.84		1.70		3.52	
	Raw	1.38	1.74	1.58	1.99	1.30	1.84	2.29	3.18	5.52	6.46
	LS	0.84	1.30	1.04	1.43	0.98	1.37	1.67	2.38	3.13	4.94
	LOCI	1.44	2.01	1.63	2.22	1.42	2.06	2.56	3.56	5.69	7.49
	PT	0.96	1.75	1.04	1.73	0.90	1.42	1.69	2.96	3.80	6.44
IPSL-CM5-LR	Obs	0.98		1.04		0.84		1.70		3.52	
	Raw	1.24	1.06	1.27	0.99	0.93	0.66	2.26	1.65	4.08	3.96
	LS	0.88	0.77	1.04	0.80	1.01	0.70	1.69	1.32	3.15	3.04
	LOCI	1.27	1.09	1.44	1.09	1.31	0.95	2.41	1.82	4.37	4.05
	PT	0.99	0.98	1.04	0.88	0.82	0.63	1.66	1.43	3.67	4.01
MIROC5	Obs	0.98		1.04		0.84		1.70		3.52	
	Raw	0.75	0.89	0.86	0.98	0.64	0.75	1.31	1.54	2.88	3.78
	LS	0.92	1.08	1.04	1.19	0.85	0.95	1.62	1.90	3.46	4.24
	LOCI	1.16	1.38	1.39	1.59	1.16	1.38	2.06	2.45	4.39	5.49
	PT	1.00	1.34	1.04	1.32	0.78	0.93	1.63	2.07	3.94	5.19
MPI-ESM-LR	Obs	0.98		1.04		0.84		1.70		3.52	
	Raw	0.81	0.93	0.78	0.78	0.58	0.48	1.36	1.27	2.80	3.54
	LS	1.10	1.18	1.05	1.01	0.86	0.61	1.74	1.67	3.85	4.71
	LOCI	1.10	1.23	1.04	1.04	0.79	0.61	1.77	1.66	3.87	4.87
	PT	1.00	1.19	1.04	1.06	0.87	0.68	1.76	1.67	3.58	4.74

W directions will be stronger during the warm phase, and it is important to link these airflows to mudflow occurrences associated with named circulation patterns in the future.

4.2. Changes in precipitation climatology experimented by CMIP5

4.2.1. Evaluation of bias correction methods applied to precipitation

The evaluation of daily mean precipitation values of GCM simulations before and after bias corrections against the observational variable at the Gallyaaraal and Sokh meteorological stations are listed in [Table 4](#) and [Table A2](#). Time-series based performances of observed precipitation, GCM outputs and corrected data are visualised as 7 days running mean to smooth daily variability of precipitation ([Figs. 8–9](#)). Additionally, Q-Q plot is used to compare the theoretical distributions of each parameter for the Gallyaaraal station ([Figs. 10 and 11](#)).

[Table 4](#) present that the raw data of the models, namely ACCESS1-0, CNRM-CM5, HadGEM2-CC, HadGEM2-ES and IPSL-CM5-LR

overestimate the average precipitation (1.84, 1.34, 1.50, 1.58, 1.27 mm each) compared to the observation (1.04 mm) for the investigation period 1979–2005 in Gallyaaraal station. In contrast, MIROC5 and MPI-ESM-LR GCMs underestimate the precipitation values (0.86 and 0.78 mm), at the same time bcc-csm1-1 (1.09 mm) slightly overestimates precipitation over the Gallyaaraal station. It is notable that mean values of raw precipitation data presented by CMCC-CM (1.04 mm) and GFDL-CM3 (1.02 mm) models are similar to the mean value (1.04 mm) of observed timeseries.

Frequency statistics of mean values at the Gallyaaraal station after the application of bias correction techniques (LS, LOCI and PT) significantly improved and had a good estimation of bias corrected precipitation values compared to the GCM raw data. Correcting the precipitation timeseries with **LS method** ensures that maximum rainfall never exceeds the raw maximums if the model raw overestimates the observed data. After correction of daily rainfall, the response of corrected values at Gallyaaraal station by scaling algorithm gives more realistic mean

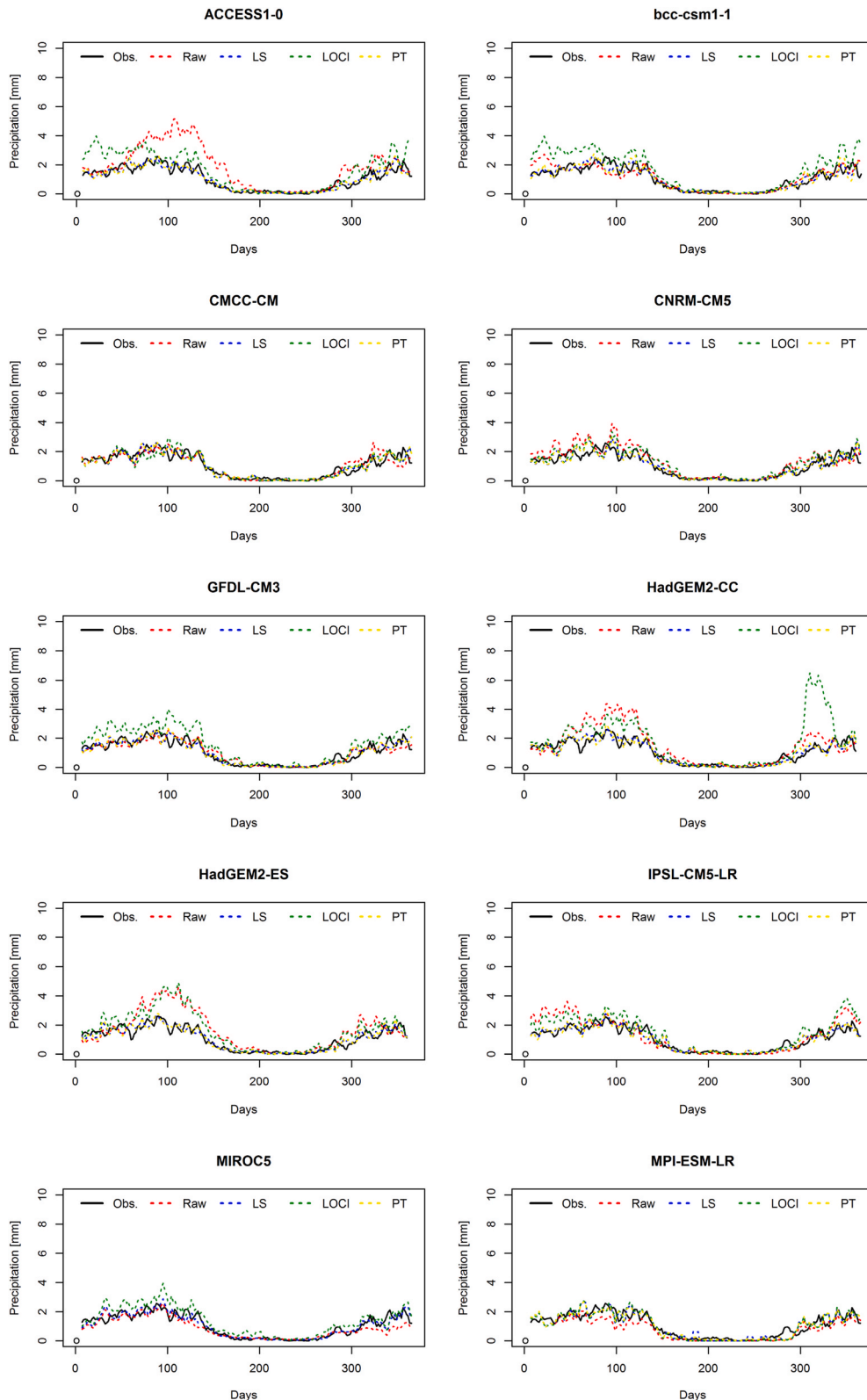


Fig. 8. Daily mean precipitation of observed, raw GCM-simulated and bias corrected values at the Gallyaarial station with the 7-day smoothed moving average method for the years of 1979–2005.

values even though the method underestimates the maximums of observed precipitation (Table 4, Figs. 8–11).

Compared to the LS method, **LOCI algorithm** significantly overestimates the GCM simulation from observation values, likewise frequency statistics of corrected values are higher than the mean values.

After the correction by LOCI procedure for the bias in the station, 27 years averaged precipitation data, it was found that it is insignificant for most of models, however, results from CMCC-CM, CNRM-CM5 and MPI-ESM-LR are more realistic (Table 4, Figs. 8–11).

The ability of **PT method** to reproduce the precipitation shows

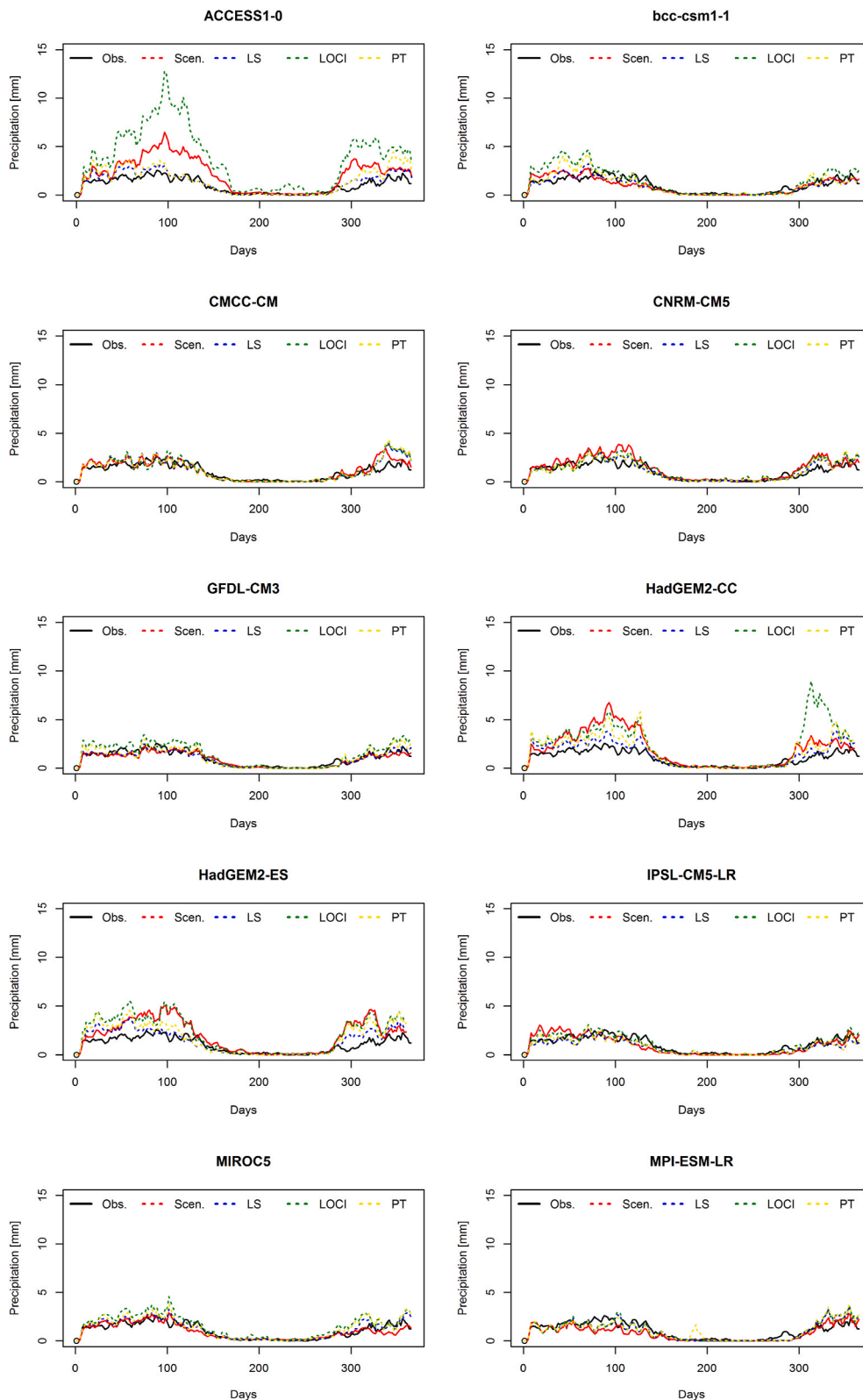


Fig. 9. Daily mean precipitation of observed, GCM raw-scenario and bias corrected values at the Gallyaaral station with the 7-day smoothed moving average method for the years of 2071–2100.

robust results amongst bias correction techniques applied in this study. Frequency statistics of mean values (Table 4 and A2) and visualisation (Figs. 8–11) perform that method fits well and improves the GCM raw data achieving close agreement of the mean corrected values with the observed timeseries.

Out of ten selected GCMs the best frequency metrics and bias corrected results are related to CMCC-CM and MPI-ESM-LR models. In a first case, the raw data of CMCC-CM model reveals similar station based timeseries with minor overestimation in the beginning of winter season (Fig. 8). For the MPI-ESM-LR model, the raw values, after applying bias

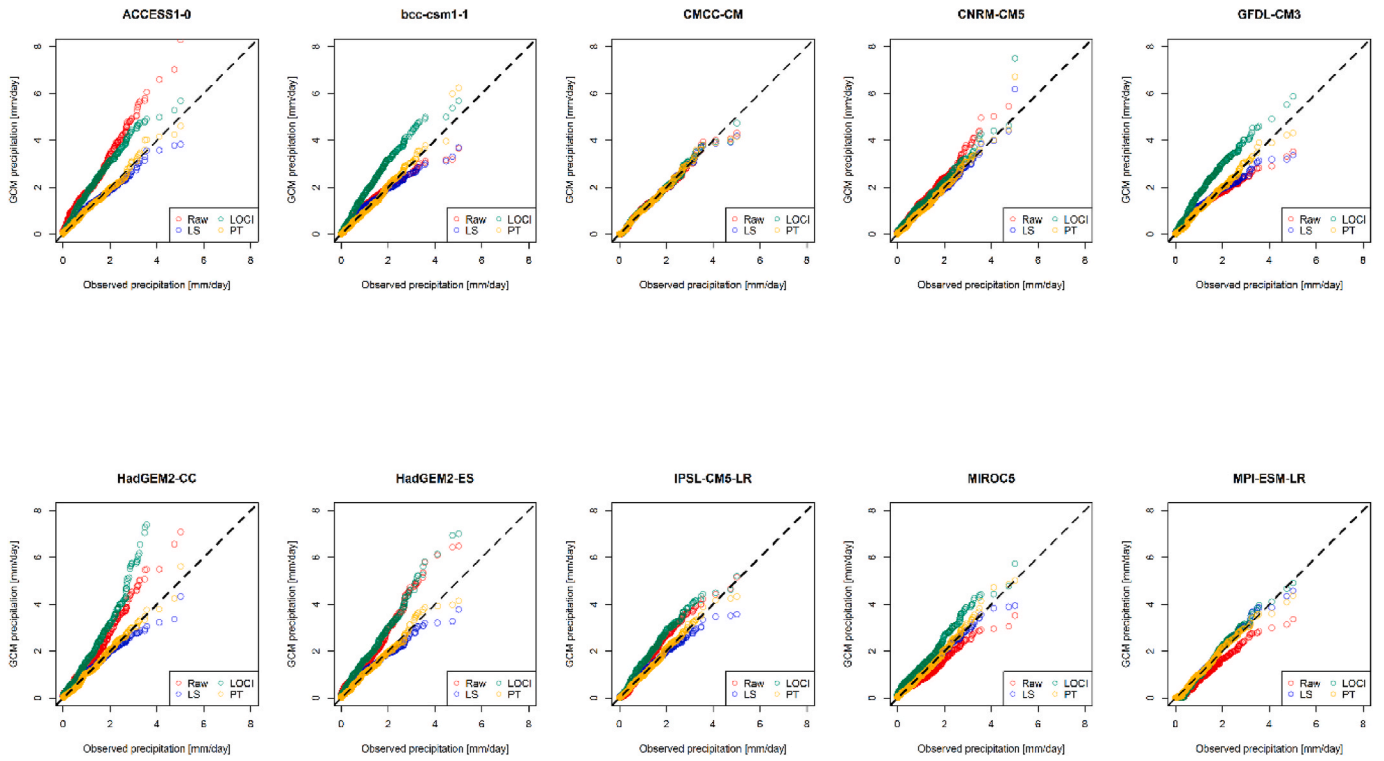


Fig. 10. Q-Q plot of corrected daily average precipitation against station (Gallyaaral) daily mean precipitation for the period of 1979–2005.

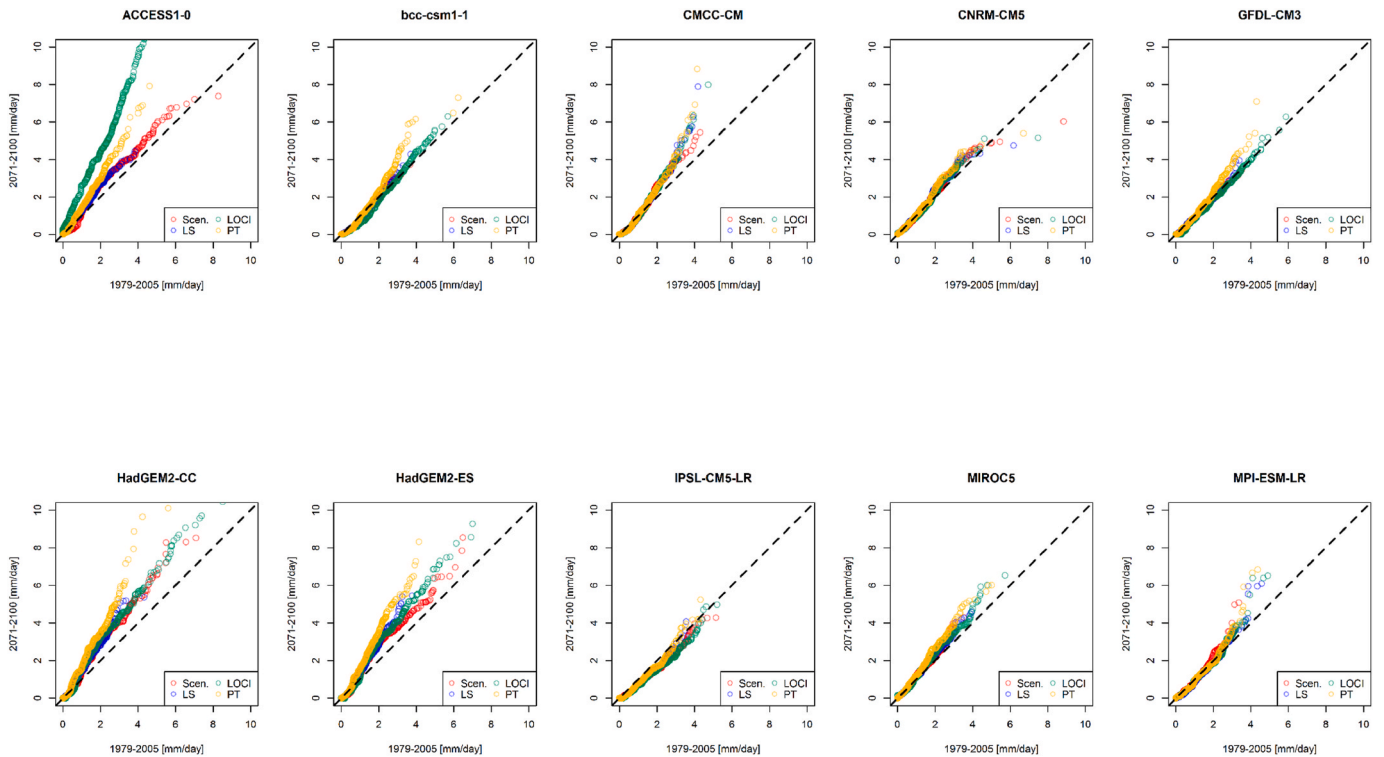


Fig. 11. Q-Q plot of corrected precipitation from selected GCMs scenarios for the period of 2071–2100.

correction techniques, match the observation variable. Hence, the above named two models' bias corrected outputs, preferably obtained by PT technique, could help to identify precipitation threshold triggering mudflows in the study area for the recent and future climate.

4.2.2. Linking global circulation model outputs to ADRM

Probabilities of mudflow occurrences using antecedent daily rainfall conditions as an independent factor triggering mudflow events has been analysed in this section. Equation (18) explained for the Gallyaaral station adapted from Mamadjanova et al. (2018) was used to calculate

Table 5

Rainfall threshold probability equations of mudflow occurrences in the Gallyaaraal station established using GCM corrected precipitation data (P – probability, r – daily rainfall, r_a –antecedent rainfall, $\text{Pr}(>\chi)$ - chi-squared results).

Time period	CMIP5 GCM	Probability equation	$\text{Pr}(>\chi)$
Control 1979–2005	CMCC-CM	$\log\left(\frac{P}{1-P}\right) = -5.62 + 0.19r + 0.10*r_a$	3.12e-13
	MPI-ESM-LR	$\log\left(\frac{P}{1-P}\right) = -4.43 + 0.17*r + 0.07*r_a$	5.25e-10
Scenario 2071- 2100	CMCC-CM	$\log\left(\frac{P}{1-P}\right) = -4.61 + 0.15*r + 0.06*r_a$	7.99e-09
	MPI-ESM-LR	$\log\left(\frac{P}{1-P}\right) = -3.86 + 0.13*r + 0.03*r_a$	0.00082

the threshold probability line for control run (1979–2005) and future scenarios (2071–2100) of two selected GCMs (CMCC-CM and MPI-ESM-LR) (Table 5). Model outputs are presented in Fig. 12.

$$\log\left(\frac{P}{1-P}\right) = -3.87 + 0.10*r + 0.05*r_a \quad (18)$$

Probability envelopes of mudflow occurrences based on model data which include antecedent rainfall condition and daily precipitation as input data for ADRM show that results using equation (18) works satisfactorily for both GCMs (Fig. 12). However, calculation of the probability line (Table 5) based on the synthetic mudflow occurrences assumed by taking into account the selected rainfall class CWT C, SW and W generating extreme events, show that CMCC-CM underestimates the 0.5 and 0.9 threshold probability lines for control run and future scenario (Fig. 12). This might be due to exclusion of information on temperature conditions as this is an important parameter to be taken into account while running the ADRM as it was discussed in Mamadjanova et al. (2018). The modelling results for MPI-ESM-LR precipitation data suggest that the probability line is underestimated (<0.5 and <0.9) for the control period, however, the probability for the future scenario fits, but has some uncertainties. This might be due to the very high values of precipitation and antecedent rainfall index projected by MPI-ESM-LR GCM. In general, both GCMs were able to capture probability lines even though the ADRM has some limitations due to the exclusion of temperature conditions. Overall the outputs from the GCMs (CMCC and MPI-ESM-LR) for the threshold probabilities are acceptable as both can capture the antecedent conditions and extreme events evaluated by ADRM taking into account CWT C, SW and NW airflows as a proxy to simulate and project future risk of mudflows in Uzbekistan.

5. Discussion

5.1. Projected CWT

The research presented in this study compared the abilities of 10 GCMs from CMIP5 multi-model projections with the aim to investigate large scale circulation and precipitation climatology as the main triggering factor of mudflow occurrences in Uzbekistan for the historical period of 1979–2005 and future scenarios under the RCP8.5 for the 2071–2100 period.

CMIP5 models are used to evaluate CWT frequencies under recent and future climate conditions to enable to link the changes in CWT to mudflow occurrences induced by precipitation associated with specific circulation patterns. Only a limited number of investigations are focused on the projected changes in atmospheric circulation over Central Asia, particularly in Uzbekistan and they must be duly taken into account to compare achieved results in this study. To our knowledge, no study has

examined the relationship between projected large-scale circulation and its impact on future mudflow risk in Uzbekistan.

The increased frequency of CWT W airflow is expected to contribute to an overall increase of precipitation by the end of the century. This outcome is corroborated by [Reyers et al. \(2013\)](#) in which ECHAM5/MPI-OM1 ensemble is dynamically downscaled by CWT approach for the Aksu River basin located in Central Asia. Moreover, this weather type gives a climate change signal in mudflow occurrences associated with the mechanism of westerly airflow in lower troposphere over the study area for the future. Conversely, the robust decrease in the occurrence of CWT AC leads to lower precipitation particularly when it is hybrid or associated with W and SW flows. Further, the smaller magnitude of ensemble mean in changes associated with CWT E, SE, S, NW and N circulation patterns show that the relationship between named weather types and precipitation has a weaker climate change signal and it is assumed to remain invariant (Tables 2–3 and Fig. 7). Similar results have been obtained by [Reyers et al. \(2013\)](#).

However, model outcomes for the CWT C strongly vary in seasonal frequencies which predict that the climate will be rainy in warm period (March–August) and mudflows associated with cyclonic days will occur frequently in comparison to the cold period (September–February) for Uzbekistan in the future. Therefore, the skill of CMIP5 models projected for CWT SW highlight that significant uncertainties exist over spring and summer even though there is a clear signal that SW will be less frequent in future autumns and winters. [Zhao et al. \(2018\)](#) confirms that subtropical westerly jet centred over Caspian Sea will change its position by shifting further south in the last 50 years of the 21st century and it will affect summer rainfall in Central Asian countries including Uzbekistan. Ensemble mean results in this study also indicate the frequency of CWT SW which brings tropical moist and warm air associated with extreme rainfall to Uzbekistan is more likely to decrease under future climate conditions. However, results in [Reyers et al. \(2013\)](#) show opposite signs in frequency of CWT SW in the future climate. This disagreement motivates a more detailed investigation in future.

Finally, the significant changes in undefined weather class especially in warm periods can be summarised by regarding the influence of orographic features of the investigation area. On the other hand, it can be attributed to outperform identified biases of individual models along with CMIP5 projection.

5.2. Projected precipitation threshold

Simulated precipitation was analysed by applying three bias correction algorithms (LS, LOCI, PT) to select suitable model outputs to run the ADRM model. Precipitation threshold triggering mudflow occurrences for the control period (1979–2005) and future scenario (2071–2100) obtained for the Gallyaaraal station were evaluated using logistic approach equation (please see [Mamadjanova et al. \(2018\)](#) for details). At the same time threshold probability was identified taking into account mudflow generating weather patterns namely CWT C, SW and W associated with daily rainfall (≤ 20 mm) and antecedent conditions (≤ 40 mm) as central proxies to simulate synthetic mudflow occurrences under the recent and future climate scenarios.

However, several limitations still exist in this study. First, amongst the ten models used only outputs from two models captured well to establish the precipitation threshold probabilities using ADRM and statistical transfer function of LRM. [Huang et al. \(2014\)](#) note for instance that out of 28 CMIP5 models only 5 models have better ability to capture a multimodel ensemble mean and simulates well rainfall observation over Central Asia and Tibetan Plateau. [Zhao et al. \(2018\)](#) also report that only 14 models of the 25 models from CMIP5 projection in which the precipitation distribution matches well with subtropical westerly jet circulation over the Central Asia. It would be desirable to run different GCMs with rainfall data and compare the achieved results in order to better understand future risk of extreme mudflow events and the triggering factors.

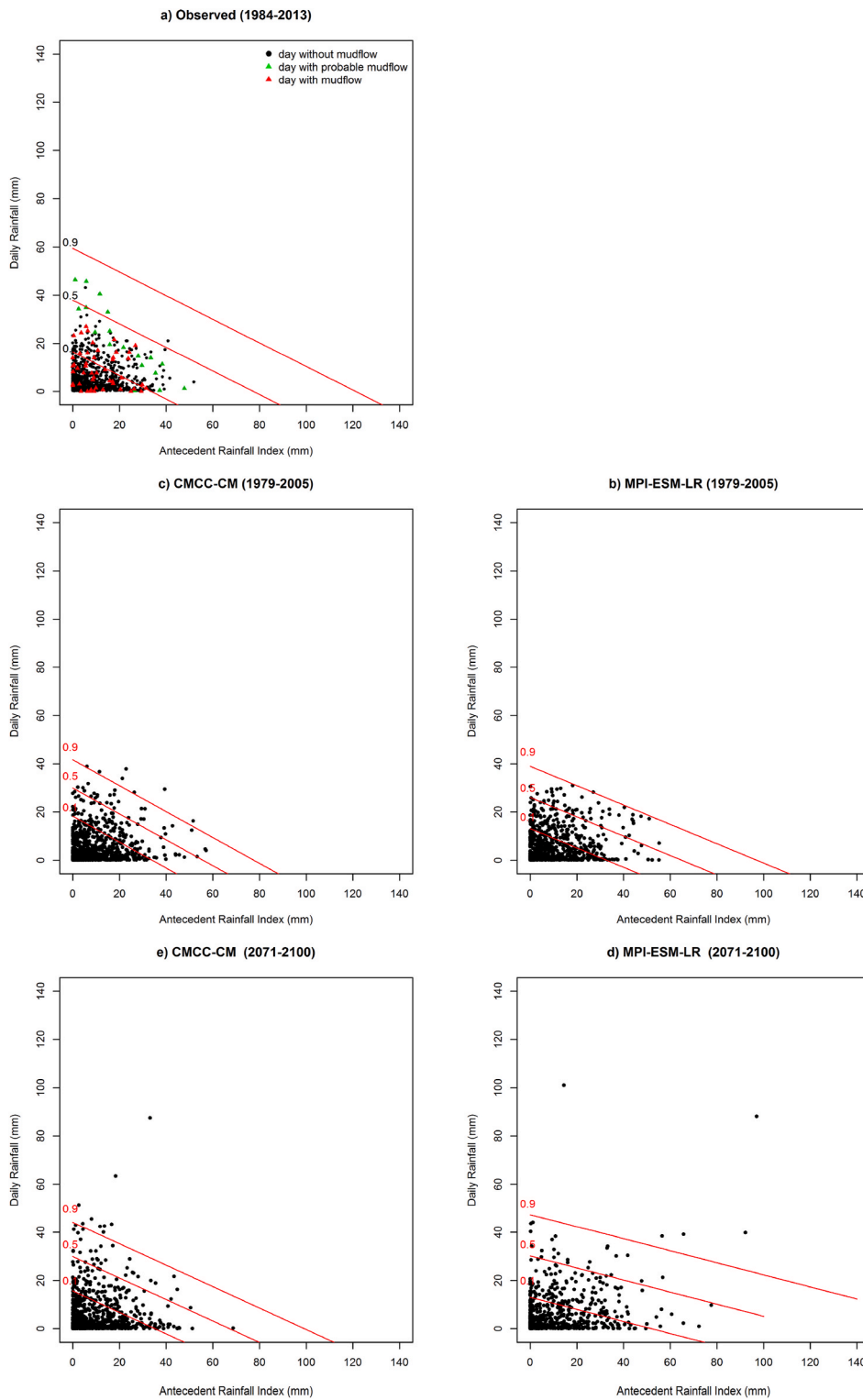


Fig. 12. ADRM applied to the observed and representative CMIP5 GCMs outputs for the Gal-lyaaral station for the March–August covering three time period: station data 1984–2013 adapted from Mamadjanova et al. (2018) (a), 1979–2005 for the control run (b, c) and 2071–2100 for future scenario (d, e). Red lines indicate the 0.1, 0.5 and 0.9 probability threshold triggering mudflow occurrences. Equation (18) and Table 5 were used for calculation of the probability lines at the selected station. (For interpretation of the references to colour in this figure legend, the reader is referred to the Web version of this article.)

Second, the synthetic or probable mudflow derived from the rainfall data on relevant day with CWT C, SW and W circulations, which are used as a proxy in this case, cannot be dated exactly for the same day of observational data. Schmidt and Glade (2003) have shared this limitation in their study. Nevertheless, the results from the use of two GCMs demonstrate reasonable outputs when compared with the thresholds obtained from observational data.

Despite all weaknesses, it can be concluded that CMIP5 GCMs precipitation timeseries with efficient downscaling and bias correction techniques can link precipitation extremes and rainfall induced landslide types using antecedent rainfall model together with logistic regression function for any region with available rainfall and landslides data.

6. Conclusion

In this study, daily mean Z_{700} and precipitation outputs from 10 GCMs of CMIP5 system have been evaluated under both current and future climate scenarios enabling better understanding of climate variability and precipitation induced natural hazards under global warming conditions in a longer timescale. Only the first member (named r1ip1) from the historical experiment (1979–2005) and future (2071–2100) under the RCP8.5 emission scenario (radiative forcing surplus of 8.5 W/m² in 2100) has been considered for each GCM.

Several conclusions can be made from the analysis done in this study:

1. Seasonal frequencies of CWTs do not change significantly as the overall results indicate that spatial frequency of airflow directions have an amplitude up to ± 5 percent in the 2071–2100 years.
2. Changed frequencies of cyclonic (C) and westerly (W) airflow directions will potentially contribute to more extreme mudflow occurrences during the warm season (March–August) by up to 5% near the end of the century 2071–2100. However, the ensemble results show uncertainties regarding the CWT SW airflow associated with the most devastating mudflow events in Uzbekistan for the projected period of March–August in 2071–2100. These uncertainties in the projected atmospheric circulations frequencies for the future climate (2071–2100) could be also attributed to the systematic errors between individual model simulations. Future research should concern on more detailed analysis of these factors in order to obtain robust estimates of climate change signal.
3. The outputs of linear scaling (LS), local intensity scaling (LOCI) and power transformation (PT) of precipitation bias correction techniques indicate that the PT approach has a higher ability to capture the observed precipitation and reproduce more realistic precipitation values from the model raw data for the historical experiments.
4. CMCC-CM and MPI-ESM-LR models, of the 10 selected GCMs of CMIP5 models, show realistic results for the historical experiments of precipitation data. Whereas CNRM-CM5, GFDL-CM3, IPS-C5M-LR and MIROC5 represent remarkable outputs for future scenarios. The remaining four models overestimate precipitation values over Uzbekistan.
5. CMCC-CM and MPI-ESM-LR model outputs corrected by PT bias technique are suitable to investigate changes in precipitation timeseries and its link to mudflow occurrences under recent and future climate conditions for the study area.
6. Threshold probability equation based on observed data works satisfactorily, however equation coefficients which are not derived from the observed data give slightly underestimated threshold lines in both GCMs (CMCC-CM and MPI-ESM-LR).

7. CWT C, SW and W airflow directions can work satisfactorily as proxies to identify precipitation threshold triggering mudflows in the study area.

8. The model outputs show that mudflow occurrences will increase by the end of the century, as the model scenarios show increasing precipitation amount in the study area.

However, several open questions still exist, and much works remain to be done to connect the results in the current study. First, decreasing of the weather circulations (e.g., SW) favourable for mudflow occurrences in Uzbekistan will assign less mudflows under this directional flow despite the overall result shows increasing of precipitation induced natural hazard by the end of the century. The reasons behind this are unclear: will SW frequency reduce due to the significant poleward movement of subtropical westerly jet as suggested by Hunt and Dimri (2021); Thapa et al. (2020) as observed in the past or propagation to south as hypothesised by Zhao et al. (2018) which could possibly increase the frequency of other circulation types (e.g., C and W) contributing to more mudflow occurrences in the future? Secondly, it will be important to explore how the large-scale circulations will impact on moisture source and flux associated with the directional flows and their relationship with extreme rainfall events initiating mudflows in a changing climate. And finally, the impact of elevated heating (Hu and Boos, 2017) by the rise of orography which has important effects on regional scale circulations, and therefore its interaction with convective precipitation in future climate scenarios need to be investigated. Furthermore it would be pertinent to explore whether this would have any relation to the rise of days with undefined weather class or is this related to model uncertainty. The interactions between all these factors could potentially lead to very strong impacts, and therefore all these caveats motivate further studies.

Author's contribution

This paper is based on the fifth and sixth chapters of the first author's PhD dissertation titled Variability of the steering factors for extreme hydrometeorological events in Central Asia and its relation to the formation of mudflows in the piedmont areas of Uzbekistan. GM and GCL jointly developed and designed the details of this research. GM performed the analyses, produced figures and wrote the first draft of the manuscript. Manuscript was edited and revised by GM and GCL.

Declaration of competing interest

The authors declare that they have no conflict of interest.: This work is a part of the first author's Ph.D. thesis titled "Variability of the steering factors for extreme hydrometeorological events in Central Asia and its relation to the formation of mudflows in the piedmont areas of Uzbekistan" at the University of Birmingham in 2019. It was declared in the Authors Contribution section and in a cover letter to Editor.

Acknowledgements

The authors special thanks are extended to Simon Wild for his contribution to the CWT methodology and Michael A Walz for his support in logistic regression algorithm. The Blue-BEAR HPC provided by the University of Birmingham has enabled to run the computational work. CMIP5 dataset used in this study were made available through the ceda.ac.uk and cera-www.dkrz.de. Authors are grateful to ECMWF for granting access to the ERA-Interim reanalysis data. First author expresses her gratitude to Islamic Development Bank (IsDB) for awarding her with a PhD scholarship at the University of Birmingham, UK.

Appendix A

Table A1

CMIP5 model acronyms, modelling centre name and acronym, experiment type, time period of data availability, model grid resolution, and a representative reference.

Model name	Model abbreviation	Climate centre	Acronym for the climate centre	Calendar	Experiment	Time period for this study		GCM resolution (lat × lon)	Reference
						control	scenario		
ACCESS1-0	Australian Community Climate and Earth-System Simulator, version 1.0	Commonwealth Scientific and industrial Research Organization/ Bureau of Meteorology, Australia	CSIO CAWCR, Australia	prolepticgregorian	RCP8.5 r1i1p1	1979–2005	2071–2100	1.9 × 1.2 L38	Bi et al. (2012)
bcc-csm1-1	Beijing Climate Centre, Climate System Model, version 1.1	Beijing Climate Centre, China Meteorological Administration, China	BCC, CMA, China	365 day	RCP8.5 r1i1p1	1979–2005	2071–2100	2.8 × 2.8 L26	Wu et al. (2014)
CMCC-CM	CMCC-CM	CMCC - Centro Euro-Mediterraneo per i Cambiamenti, Italy	CMCC, Italia	standard	RCP8.5 r1i1p1	1979–2005	2071–2100	0.75 × 0.75 L31	Scoccimarro et al. (2011)
CNRM-CM5	Centre National de Recherches Météorologiques Coupled Global Climate Model, version 5	Centre National de Recherches Météorologiques (CNRM), France and Centre European de Recherches et de Formation Avancée en Calcul Scientifique (CERFACS), France	CNRM-CERFACS, France	standard	RCP8.5 r1i1p1	1979–2005	2071–2100	1.4 × 1.4 L31	Voltaire et al. (2013)
GFDL-CM3	Geophysical Fluid Dynamics Laboratory Climate Model, version 3	Geophysical Fluid Dynamics Laboratory (GFDL) at National Oceanic and Atmospheric Administration (NOAA)	NOAA-GFDL, United States	365 day	RCP8.5 r1i1p1	1979–2005	2071–2100	2.5 × 2.0 L48	Donner et al. (2011)
HadGEM2-CC	Hadley Centre Global Environment Model, version 2, Carbon Cycle	Met Office Hadley Centre, United Kingdom	MOHC, UK	360 day	RCP8.5 r1i1p1	1979–2005	2071–2100	1.9 × 1.2 L60	Martin et al. (2011)
HadGEM2-ES	Hadley Centre Global Environment Model, version 2, Earth System	Met Office Hadley Centre, United Kingdom	MOHC, UK	360 day	RCP8.5 r1i1p1	1979–2005	2071–2099		Jones et al. (2011)
IPSL-CM5A-LR	L'Institut Pierre-Simon Laplace Coupled Model, version 5 A, low resolution	Institute Pierre Simon Laplace, France	IPSL, France	365 day	RCP8.5 r1i1p1	1979–2005	2071–2100	3.7 × 1.9 L39	Dufresne et al. (2013)
MIROC5	Model for Interdisciplinary Research on Climate, version 5	Atmosphere and Ocean Research Institute (The University of Tokyo), National Institute for Environmental Studies, and Japan Agency for Marine-Earth Science and Technology, Japan	AORI-NIES/JAMSTEC, Japan	standard	RCP8.5 r1i1p1	1979–2005	2071–2100	1.4 × 1.4 L40	Watanabe et al. (2011)
MPI-ESM-LR	Max Planck Institute Earth System Model, low resolution	Max Planck Institute for Meteorology, Germany	MPI-N, Germany	prolepticgregorian	RCP8.5 r1i1p1	1979–2005	2071–2100	1.9 × 1.9 L47	Zanchettin et al. (2013)

Table A2

Frequency based statistics (unit: mm) of daily mean observed precipitation, GCM raw data and bias-corrected values (LS, LOCI, PT) at the Sokh station for the historical period (1979–2005) and the future scenario (2071–2100).

		standard deviation		mean		median		75th percentile		99th percentile	
		control	scenario	control	scenario	control	scenario	control	scenario	control	scenario
ACCESS1-0	Obs	0.72		0.96		0.80		1.29		3.14	
	Raw	1.49	1.49	2.16	2.20	1.62	1.78	3.09	3.23	6.02	6.05
	LS	0.52	0.64	0.96	1.04	0.83	0.99	1.31	1.50	2.18	2.66
	LOCI	1.39	1.50	1.95	2.14	1.59	1.96	2.62	3.21	6.16	5.99
	PT	0.68	1.13	0.96	1.35	0.79	1.05	1.32	1.97	3.10	4.67
bcc-csm1-1	Obs	0.72		0.96		0.80		1.29		3.14	
	Raw	0.96	1.04	1.51	1.44	1.59	1.55	2.24	2.30	3.41	3.60
	LS	0.55	0.49	0.96	0.84	0.84	0.76	1.24	1.18	2.61	2.00
	LOCI	1.18	1.29	1.91	1.84	1.70	1.74	2.76	2.86	4.77	4.72
	PT	0.80	0.86	0.96	1.02	0.71	0.79	1.31	1.57	3.87	3.73
CMCC-CM	Obs	0.72		0.96		0.80		1.29		3.14	
	Raw	1.87	2.07	2.14	2.33	1.72	2.05	2.98	3.69	7.89	7.79
	LS	0.70	0.73	0.96	0.94	0.88	0.88	1.29	1.45	3.09	2.65
	LOCI	0.93	1.11	1.24	1.33	1.11	1.16	1.71	2.10	3.73	4.18
	PT	0.78	1.02	0.96	1.11	0.82	0.90	1.35	1.76	3.48	4.06
CNRM-CM5	Obs	0.72		0.96		0.80		1.29		3.14	
	Raw	1.11	1.32	2.00	2.22	1.77	1.94	2.63	3.24	5.39	5.67
	LS	0.54	0.67	0.96	1.08	0.85	0.97	1.32	1.61	2.58	2.79
	LOCI	0.87	1.02	1.50	1.66	1.35	1.47	2.04	2.49	4.05	3.89
	PT	0.71	0.90	0.96	1.15	0.82	0.97	1.34	1.79	3.41	3.80
GFDL-CM3	Obs	0.72		0.96		0.80		1.29		3.14	
	Raw	1.42	1.46	2.07	2.04	2.08	2.04	3.03	3.06	5.24	5.50
	LS	0.55	0.60	0.96	0.96	0.86	0.86	1.24	1.37	2.54	2.30
	LOCI	1.18	1.33	1.84	1.99	1.80	1.95	2.52	2.85	5.20	5.04
	PT	0.77	1.04	0.96	1.20	0.79	0.96	1.36	1.75	3.55	4.78
HadGEM2-CC	Obs	0.72		0.96		0.80		1.29		3.14	
	Raw	1.31	1.44	1.96	2.08	1.49	1.79	2.84	3.10	5.29	5.76
	LS	0.51	0.66	0.96	1.07	0.89	1.06	1.34	1.57	2.23	2.61
	LOCI	1.27	1.49	1.90	2.17	1.60	2.06	2.73	3.16	5.48	5.85
	PT	0.77	1.19	0.96	1.38	0.80	1.21	1.27	1.96	3.34	5.09
HadGEM2-ES	Obs	0.72		0.96		0.80		1.29		3.14	
	Raw	1.46	1.44	2.08	2.18	1.55	1.96	3.15	3.19	5.93	5.74
	LS	0.49	0.64	0.96	1.07	0.88	1.07	1.31	1.53	2.18	2.54
	LOCI	1.54	1.55	2.09	2.34	1.63	2.21	2.77	3.34	6.65	6.13
	PT	0.72	1.39	0.96	1.56	0.79	1.30	1.26	2.27	3.31	5.92
IPSL-CM5-LR	Obs	0.72		0.96		0.80		1.29		3.14	
	Raw	1.27	1.31	2.28	1.84	2.40	1.98	3.21	2.91	4.81	4.47
	LS	0.54	0.53	0.96	0.72	0.85	0.64	1.28	1.04	2.42	2.15
	LOCI	1.19	1.28	1.94	1.65	1.94	1.60	2.75	2.60	4.83	4.85
	PT	0.80	1.07	0.96	0.96	0.75	0.67	1.42	1.38	3.46	4.60
MIROC5	Obs	0.72		0.96		0.80		1.29		3.14	
	Raw	1.34	1.73	2.28	2.61	2.07	2.61	3.17	3.87	5.55	6.86
	LS	0.52	0.68	0.96	1.06	0.88	0.91	1.27	1.29	2.51	3.37
	LOCI	0.95	1.25	1.70	2.00	1.66	1.82	2.26	2.67	4.17	5.81
	PT	0.70	1.15	0.96	1.33	0.83	1.04	1.31	1.79	3.17	5.14
MPI-ESM-LR	Obs	0.72		0.96		0.80		1.29		3.14	
	Raw	1.78	1.93	2.29	2.34	2.30	2.38	3.53	3.69	6.38	7.19
	LS	0.78	0.86	0.96	0.92	0.83	0.85	1.26	1.26	3.44	3.09
	LOCI	1.01	1.21	1.40	1.50	1.30	1.40	2.05	2.25	3.82	4.47
	PT	0.83	1.00	0.96	1.11	0.77	0.93	1.31	1.66	3.47	3.93

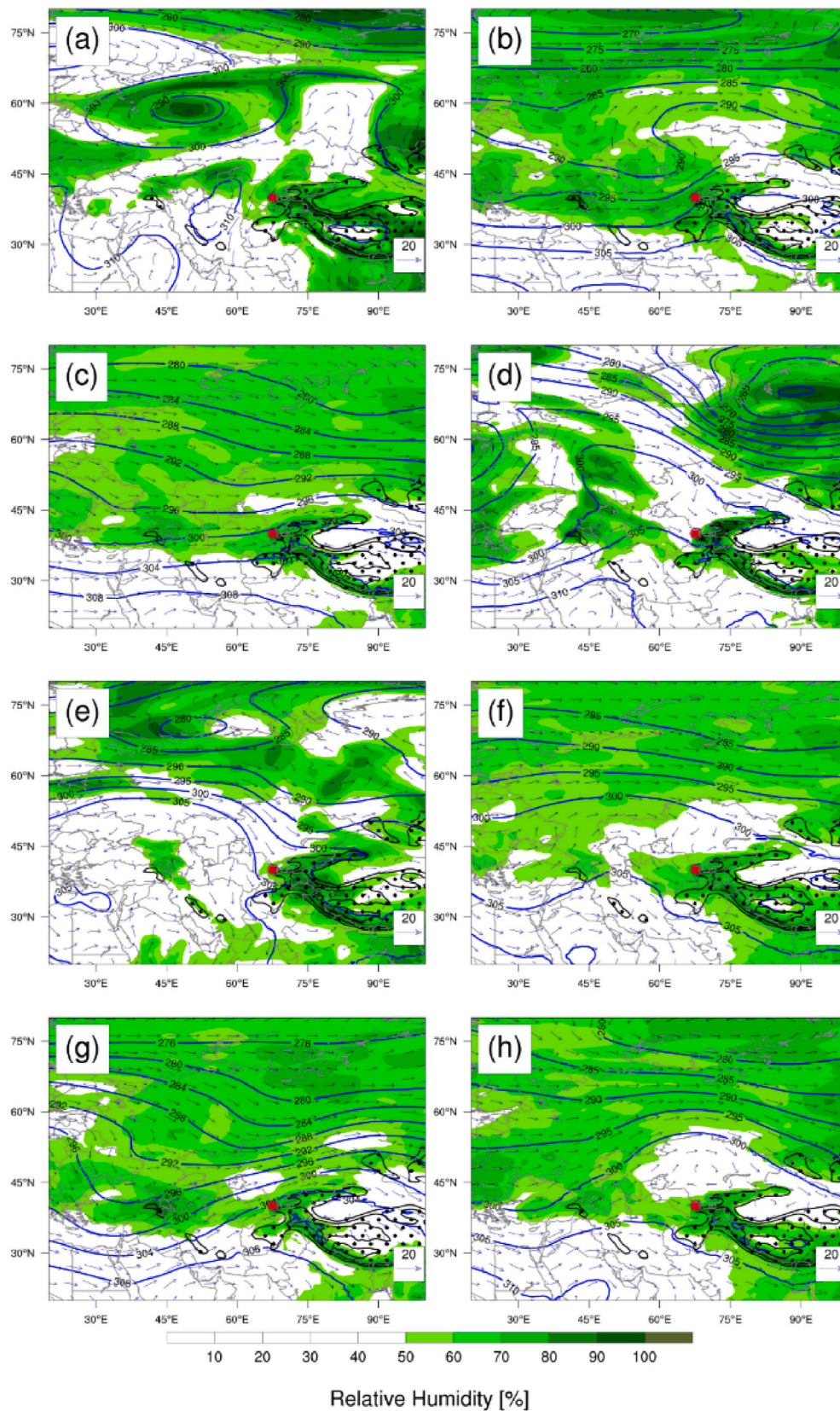


Fig. A1. CWT north-east (a), south-west (b), west (c), north-west (d), north (e), cyclonic (f), anticyclonic (g) and undefined (h) weather type characteristics on the mudflow days occurring in Uzbekistan for the period of 1984–2013. ERA-Interim 700 hPa geopotential height, relative humidity and wind component were used to produce this figure. Red circle indicates the central grid point (40.0°N-67.5°E). Black contour lines together with black dots show the area where the topography is above 2000 m further corresponding 3000 and 4000 m..

References

- Babko, V.L., 1978. Mudflow hazards in Uzbekistan. In: Proceedings of XV Scientific Conference on Debris Flows. Tashkent, September, pp. 27–29.
- Bi, D., Dix, M., Marsland, S., O'farrell, S., Rashid, H., Uotila, P., Hirst, A., Kowalczyk, E., Golebiewski, M., Sullivan, A., Yan, Hannah, Franklin, C., Sun, Vohralik, Watterson, Zhou, K., Fiedler, R., Collier, M., Puri, K., 2012. The ACCESS Coupled Model: Description, Control Climate and Evaluation.
- Bobojonov, I., Aw-Hassan, A., 2014. Impacts of climate change on farm income security in Central Asia: an integrated modeling approach. *Agric. Ecosyst. Environ.* 188, 245–255.
- Brigode, P., Gérardin, M., Bernardara, P., Gailhard, J., Ribstein, P., 2018. Changes in French weather pattern seasonal frequencies projected by a CMIP5 ensemble. *Int. J. Climatol.* 38 (10), 3991–4006. <https://doi.org/10.1002/joc.5549>.
- Chiang, S.-H., Chang, K.-T., 2011. The potential impact of climate change on typhoon-triggered landslides in Taiwan, 2010–2099. *Geomorphology* 133, 143–151.
- Chub, V.Y., 2007. Climate Change Impacts on Hydrometeorological Processes, Agriculture and Water Resources of Uzbekistan. *Voris Nashriyot*, Tashkent (in Russian).
- Chub, V.Y., Trofimov, G.N., Merkushkin, A.S., 2007. Mudflows in Uzbekistan (in Russian). *Uzhydromet*, Tashkent.
- Crozier, M.J., Eyles, R.J., 1980. Assessing the probability of rapid mass movement. In: Third Australia - New Zealand Conference on Geomechanics, vol. 2. New Zealand Institution of Engineers, Wellington, 47–2.51.
- Dee, D.P., Uppala, S.M., Simmons, A.J., Berrisford, P., Poli, P., Kobayashi, S., Andrae, U., Balmaseda, M.A., Balsamo, G., Bauer, P., Bechtold, P., Beljaars, A.C.M., Van De Berg, L., Bidlot, J., Bormann, N., Delsol, C., Dragani, R., Fuentes, M., Geer, A.J., Haimberger, L., Healy, S.B., Hersbach, H., Hólm, E.V., Isaksen, I., Kållberg, P., Köhler, M., Matricardi, M., McNally, A.P., Monge-Sanz, B.M., Morcrette, J.-J., Park, B.-K., Peubey, C., De Rosnay, P., Tavolato, C., Thépaut, J.-N., Vitart, F., 2011. The ERA-Interim reanalysis: configuration and performance of the data assimilation system. *Q. J. R. Meteorol. Soc.* 137, 553–597.
- Donner, L.J., Wyman, B.L., Hemler, R.S., Horowitz, L.W., Ming, Y., Zhao, M., Golaz, J.-C., Ginoux, P., Lin, S.-J., Schwarzkopf, M.D., Austin, J., Alaka, G., Cooke, W.F., Delworth, T.L., Freidenreich, S.M., Gordon, C.T., Griffies, S.M., Held, I.M., Hurlin, W.J., Klein, S.A., Knutson, T.R., Langenhorst, A.R., Lee, H.-C., Lin, Y., Magi, B.I., Malyshev, S.L., Milly, P.C.D., Naik, V., Nath, M.J., Pincus, R., Ploshay, J. J., Ramaswamy, V., Soman, C.J., Shevliakova, E., Sirutis, J.J., Stern, W.F., Stouffer, R.J., Wilson, R.J., Winton, M., Wittenberg, A.T., Zeng, F., 2011. The dynamical core, physical parameterizations, and basic simulation characteristics of the atmospheric component AM3 of the GFDL global coupled model CM3. *J. Clim.* 24, 3484–3519.
- Dufresne, J.-L., Foujols, M.-A., Denvil, S., Caubel, A., Marti, O., Aumont, O., Balkanski, Y., Bekki, S., Bellenger, H., Benshila, R., Bony, S., Bopp, L., Braconnot, P., Brockmann, P., Cadule, P., Cheruy, F., Codron, F., Cozic, A., Cugnet, D., De Noblet, N., Duvel, J.-P., Ethé, C., Fairhead, L., Fichet, T., Flavoni, S., Friedlingstein, P., Grandpeix, J.-Y., Guez, L., Guilyardi, E., Hauglustaine, D., Hourdin, F., Idelkadi, A., Ghattas, J., Joussaume, S., Kageyama, M., Krinner, G., Labetoulle, S., Lahellec, A., Lefebvre, M.-P., Lefevre, F., Levy, C., Li, Z.X., Lloyd, J., Lott, F., Madec, G., Mancip, M., Marchand, M., Masson, S., Meurdesoif, Y., Mignot, J., Musat, I., Parouty, S., Polcher, J., Rio, C., Schulz, M., Swingedouw, D., Szopa, S., Talandier, C., Terray, P., Viovy, N., Vuichard, N., 2013. Climate change projections using the IPSL-CM5 earth system model: from CMIP3 to CMIP5. *Clim. Dynam.* 40, 2123–2165.
- El Kenawy, A.M., McCabe, M.F., 2016. Future projections of synoptic weather types over the Arabian Peninsula during the twenty-first century using an ensemble of CMIP5 models. *Theor. Appl. Climatol.* 1–17.
- Fang, G.H., Yang, J., Chen, Y.N., Zammit, C., 2015. Comparing bias correction methods in downscaling meteorological variables for a hydrologic impact study in an arid area in China. *Hydrol. Earth Syst. Sci.* 19, 2547–2559.
- Fowler, H.J., Blenkinsop, S., Tebaldi, C., 2007. Linking climate change modelling to impacts studies: recent advances in downscaling techniques for hydrological modelling. *Int. J. Climatol.* 27, 1547–1578.
- Gariano, S.L., Guzzetti, F., 2016. Landslides in a changing climate. *Earth Sci. Rev.* 162, 227–252.
- Gariano, S.L., Guzzetti, F., 2021. Mass-Movements and Climate Change. Reference Module in Earth Systems and Environmental Sciences. Elsevier.
- Glade, T., Crozier, M., Smith, P., 2000. Applying probability determination to refine landslide-triggering rainfall thresholds using an empirical "antecedent daily rainfall model". *Pure Appl. Geophys.* 157, 1059–1079.
- Hosmer, D., Lemeshow, S., 2000. Applied Logistic Regression. John Wiley & Sons, Inc, New York.
- Hu, S., Boos, W.R., 2017. Competing effects of surface albedo and orographic elevated heating on regional climate. *Geophys. Res. Lett.* 44, 6966–6973.
- Huang, A., Zhou, Y., Zhang, Y., Huang, D., Zhao, Y., Wu, H., 2014. Changes of the annual precipitation over central Asia in the twenty-first century projected by multimodels of CMIP5. *J. Clim.* 27, 6627–6646.
- Hunt, K.M.R., Dimri, A.P., 2021. Synoptic-scale precursors of landslides in the western Himalaya and Karakoram. *Sci. Total Environ.* 776, 145895.
- Isakova, A.Y., Trofimov, G.N., Mamadjanova, G., 2009. Study and Mapping of Mudflows in Uzbekistan. Scientific-Methodological Foundations of Making the National Atlas of Uzbekistan. National University of Uzbekistan, Tashkent, pp. 141–142 (in Russian).
- Jones, C.D., Hughes, J.K., Bellouin, N., Hardiman, S.C., Jones, G.S., Knight, J., Liddicoat, S., O'connor, F.M., Andres, R.J., Bell, C., Boo, K.O., Bozzo, A., Butchart, N., Cadule, P., Corbin, K.D., Doutriaux-Boucher, M., Friedlingstein, P., Gornall, J., Gray, L., Halloran, P.R., Hurtt, G., Ingram, W.J., Lamarque, J.F., Law, R. M., Meinshausen, M., Osprey, S., Palin, E.J., Parsons Chini, L., Raddatz, T., Sanderson, M.G., Sellar, A.A., Schurer, A., Valdes, P., Wood, N., Woodward, S., Yoshioka, M., Zerroukat, M., 2011. The HadGEM2-ES implementation of CMIP5 centennial simulations. *Geosci. Model Dev. (GMD)* 4, 543–570.
- Jones, P.D., Hulme, M., Briffa, K.R., 1993. A comparison of Lamb circulation types with an objective classification scheme. *Int. J. Climatol.* 13, 655–663.
- Juliev, M., Mergili, M., Mondal, I., Nurtaev, B., Pulatov, A., Hübl, J., 2019. Comparative analysis of statistical methods for landslide susceptibility mapping in the Bostanlik District, Uzbekistan. *Sci. Total Environ.* 653, 801–814.
- Karpov, P.M., Pushkarenko, V.P., 1968. Geological zonation of mudflow areas in the river basins of Uzbekistan. In: Conference Proceedings (in Russian). Samarkand.
- Karpov, P.M., Pushkarenko, V.P., Umarov, A.Y., Xodjayev, S.K., 1976. Mudflow Hazards in Uzbekistan. Fan, Tashkent, p. 134 (in Russian).
- Kure, S., Jang, S., Ohara, N., Kavvas, M.L., Chen, Z.Q., 2013. Hydrologic impact of regional climate change for the snowed and glaciered river basins in the Republic of Tajikistan: hydrological response of flow to climate change. *Hydrol. Process.* 27, 4057–4070.
- Lamb, H.H., 1972. British Isles weather types and a register of the daily sequence of circulation patterns, 1861–1971. *Geophys. Mem.* 116 (2).
- Lenderink, G., Buishand, A., Van Deursen, W., 2007. Estimates of future discharges of the river Rhine using two scenario methodologies: direct versus delta approach. *Hydrol. Earth Syst. Sci.* 11, 1145–1159.
- Lyakhovskaya, L.F., 1989. Mudflow Hazards and its Short-Term Forecasting in the Piedmont Areas of Uzbekistan (In Russian). Dissertation on the Candidate of Geographical Sciences. Central Asian Hydrometeorological Scientific Research Institute, Tashkent.
- Malsy, M., Aus Der Beeck, T., Eisner, S., Flörke, M., 2012. Climate change impacts on Central Asian water resources. *Adv. Geosci.* 32, 77–83.
- Mamadjanova, G., Wild, S., Walz, M.A., Leckebusch, G.C., 2018. The role of synoptic processes in mudflow formation in the piedmont areas of Uzbekistan. *Nat. Hazards Earth Syst. Sci.* 18, 2893–2919.
- Mannig, B., Müller, M., Starke, E., Merckenschlager, C., Mao, W., Zhi, X., Podzun, R., Jacob, D., Paeth, H., 2013. Dynamical downscaling of climate change in Central Asia. *Global Planet. Change* 110, 26–39.
- Maraun, D., Widmann, M., 2018. Statistical Downscaling and Bias Correction for Climate Research. Cambridge University Press, Cambridge.
- Martin, G.M., Bellouin, N., Collins, W.J., Culverwell, I.D., Halloran, P.R., Hardiman, S.C., Hinton, T.J., Jones, C.D., McDonald, R.E., McLaren, A.J., O'connor, F.M., Roberts, M. J., Rodriguez, J.M., Woodward, S., Best, M.J., Brooks, M.E., Brown, A.R., Butchart, N., Dearden, C., Derbyshire, S.H., Dharsai, I., Doutriaux-Boucher, M., Edwards, J.M., Falloon, P.D., Gedney, N., Ghar, L.J., Hewitt, H.T., Hobson, M., Huddleston, M.R., Hughes, J., Ineson, S., Ingram, W.J., James, P.M., Johns, T.C., Johnson, C.E., Jones, A., Jones, C.P., Joshi, M.M., Keen, A.B., Liddicoat, S., Lock, A. P., Maidens, A.V., Manners, J.C., Milton, S.F., Rae, J.G.L., Ridley, J.K., Sellar, A., Senior, C.A., Totterdell, L.J., Verhoef, A., Vidale, P.L., Wiltshire, A., 2011. The HadGEM2 family of met office unified model climate configurations. *Geosci. Model Dev. (GMD)* 4, 723–757.
- Ozturk, T., Altinsoy, H.A., Türkeş, M., Kurnaz, M.L., 2012. Simulation of temperature and precipitation climatology for the Central Asia CORDEX domain using RegCM 4.0. *Clim. Res.* 52, 63–76.
- Ozturk, T., Turp, M.T., Türkeş, M., Kurnaz, M.L., 2017. Projected changes in temperature and precipitation climatology of Central Asia CORDEX Region 8 by using RegCM4.3.5. *Atmos. Res.* 183, 296–307.
- Radchenko, I., Dervede, Y., Mannig, B., Frede, H.-G., Breuer, L., 2017. Climate change impacts on runoff in the Fergana valley (central Asia). *Water Resour.* 44, 707–730.
- Reyers, M., Pinto, J.G., Paeth, H., 2013. Statistical-dynamical downscaling of present day and future precipitation regimes in the Aksu river catchment in Central Asia. *Global Planet. Change* 107, 36–49.
- Salikhova, D.H., 1975. Aero Synoptic Conditions for Triggerring Floods in Mountain Rivers and Prediction the Floods for Fergana Valley and Kashkadarya Basin (In Russian). Dissertation on the Candidate of Geographical Sciences. Central Asian Hydrometeorological Scientific Research Institute, Tashkent.
- Santos, J.A., Belo-Pereira, M., Fraga, H., Pinto, J.G., 2016. Understanding climate change projections for precipitation over western Europe with a weather typing approach. *J. Geophys. Res.: Atmosphere* 121, 1170–1189.
- Schmidli, J., Frei, C., Vidale, P.L., 2006. Downscaling from GCM precipitation: a benchmark for dynamical and statistical downscaling methods. *Int. J. Climatol.* 26, 679–689.
- Schmidt, M., Dehn, M., 2000. Examining links between climate change and landslide activity using GCMS. In: MCLAREN, S.J., KNIVETON, D.R. (Eds.), Linking Climate Change to Land Surface Change. Springer Netherlands, Dordrecht.
- Schmidt, M., Glade, T., 2003. Linking global circulation model outputs to regional geomorphic models: a case study of landslide activity in New Zealand. *Clim. Res.* 25, 135–150.
- Scoccimarro, E., Gualdi, S., Bellucci, A., Sanna, A., Fogli, P.G., Manzini, E., Vichi, M., Oddo, P., Navarra, A., 2011. Effects of tropical cyclones on ocean heat transport in a high-resolution coupled general circulation model. *J. Clim.* 24, 4368–4384.
- Shresta, M., 2015. Data Analysis Relied on Power Transformation of Rainfall Bias Correction (V.2.0) Microsoft Excel File.
- Sommer, R., Glazirina, M., Yuldashev, T., Otarov, A., Ibraeva, M., Martynova, L., Bekenov, M., Kholov, B., Ibragimov, N., Kobilov, R., Karaev, S., Sulstonov, M., Khasanova, F., Esanbekov, M., Mavlyanov, D., Isaev, S., Abdurahimov, S., Ikrarov, R., Shezdyukova, L., De Pauw, E., 2013. Impact of climate change on wheat productivity in Central Asia. *Agric. Ecosyst. Environ.* 178, 78–99.

- Sorg, A., Bolch, T., Stoffel, M., Solomina, O., Beniston, M., 2012. Climate change impacts on glaciers and runoff in Tien Shan (Central Asia). *Nat. Clim. Change* 2, 725–731.
- Sorg, A., Huss, M., Rohrer, M., Stoffel, M., 2014. The days of plenty might soon be over in glacierized Central Asian catchments. *Environ. Res. Lett.* 9, 104018.
- Taylor, K.E., Stouffer, R.J., Meehl, G.A., 2012. An overview of CMIP5 and the experiment design. *Bull. Am. Meteorol. Soc.* 93, 485–498.
- Teutschbein, C., Seibert, J., 2012. Bias correction of regional climate model simulations for hydrological climate-change impact studies: review and evaluation of different methods. *J. Hydrol.* 456–457, 12–29.
- Thapa, U.K., St George, S., Trouet, V., 2020. Poleward excursions by the Himalayan subtropical jet over the past four centuries. *Geophys. Res. Lett.* 47, e2020GL089631.
- Trofimov, G.N., 2006. Mudflows in Uzbekistan, Prediction of Catastrophic Failure and Return Period of Mudflows in the Region under the Climate Change and Adaptation Measures (in Russian). National University of Uzbekistan, Tashkent.
- Voltaire, A., Sanchez-Gomez, E., Salas Y Méria, D., Decharme, B., Cassou, C., Sénési, S., Valcke, S., Beau, I., Alias, A., Chevallier, M., Déqué, M., Deshayes, J., Douville, H., Fernandez, E., Madec, G., Maisonnave, E., Moine, M.-P., Planton, S., Saint-Martin, D., Szopa, S., Tyteca, S., Alkama, R., Belamari, S., Braun, A., Coquart, L., Chauvin, F., 2013. The CNRM-CM5.1 global climate model: description and basic evaluation. *Clim. Dynam.* 40, 2091–2121.
- Watanabe, S., Hajima, T., Sudo, K., Nagashima, T., Takemura, T., Okajima, H., Nozawa, T., Kawase, H., Abe, M., Yokohata, T., Ise, T., Sato, H., Kato, E., Takata, K., Emori, S., Kawamiya, M., 2011. MIROC-ESM 2010: model description and basic results of CMIP5-20c3m experiments. *Geosci. Model Dev. (GMD)* 4, 845–872.
- White, C.J., Tanton, T.W., Rycroft, D.W., 2014. The impact of climate change on the water resources of the Amu Darya basin in central Asia. *Water Resour. Manag.* 28, 5267–5281.
- Wilks, D.S., 2011. *Statistical Methods in the Atmospheric Sciences*. Academic press.
- Wu, T., Song, L., Li, W., Wang, Z., Zhang, H., Xin, X., Zhang, Y., Zhang, L., Li, J., Wu, F., Liu, Y., Zhang, F., Shi, X., Chu, M., Zhang, J., Fang, Y., Wang, F., Lu, Y., Liu, X., Wei, M., Liu, Q., Zhou, W., Dong, M., Zhao, Q., Ji, J., Li, L., Zhou, M., 2014. An overview of BCC climate system model development and application for climate change studies. *J. Meteorol. Res.* 28, 34–56.
- Xenarios, S., Gafurov, A., Schmidt-Vogt, D., Sehring, J., Manandhar, S., Hergarten, C., Shigaeva, J., Foggin, M., 2018. Climate change and adaptation of mountain societies in Central Asia: uncertainties, knowledge gaps, and data constraints. *Reg. Environ. Change* 19, 1339–1352.
- Zanchettin, D., Rubino, A., Matei, D., Bothe, O., Jungclaus, J.H., 2013. Multidecadal-to-centennial SST variability in the MPI-ESM simulation ensemble for the last millennium. *Clim. Dynam.* 40, 1301–1318.
- Zhao, Y., Yu, X., Yao, J., Dong, X., 2018. Evaluation of the subtropical westerly jet and its effects on the projected summer rainfall over central Asia using multi-CMIP5 models. *Int. J. Climatol.* 38, 1176–1189.